Climate Risk Management 44 (2024) 100602

Contents lists available at ScienceDirect

Climate Risk Management

journal homepage: www.elsevier.com/locate/crm

Quantifying overheating risk in English schools: A spatially coherent climate risk assessment

Laura C. Dawkins [a,*], Kate Brown [a], Dan J. Bernie [a,b], Jason A. Lowe [a,c], Theodoros Economou [d], Duncan Grassie [e], Yair Schwartz [e], Daniel Godoy-Shimizu [e], Ivan Korolija [e], Dejan Mumovic [e], David Wingate [f], Emma Dyer [a]

[a] Met Office, Fitzroy Road, Exeter, Devon EX1 3PB, United Kingdom
[b] Faculty of Health and Life Sciences, University of Bristol, Bristol, United Kingdom
[c] Priestley International Centre for Climate, University of Leeds, Leeds, United Kingdom
[d] Climate and Atmosphere Research Center, The Cyprus Institute, Cyprus
[e] University College London, Institute of Environmental Design and Engineering, United Kingdom
[f] Department for Education, Great Smith Street, London, United Kingdom

ARTICLE INFO

Keywords:
Climate risk
Spatial risk assessment framework
Generalised additive modelling
Uncertainty quantification
Heat-stress
Overheating in buildings

ABSTRACT

Climate adaptation decision making can be informed by a quantification of current and future climate risk. This is important for understanding which populations and/or infrastructures are most at risk in order to prioritise adaptation action. When assessing the risk of overheating in buildings, many studies use advanced building models to comprehensively represent the vulnerability of the building to overheating, but often use a limited representation of the meteorological (hazard) information which does not vary realistically in space. An alternative approach for quantifying risk is to use a spatial risk assessment framework which combines information about hazard, exposure and vulnerability to estimate risk in a spatially consistent way, allowing for risk to be compared across different locations. Here we present a novel application of an open-source CLIMADA-based spatial risk assessment framework to an ensemble of climate projections to assess overheating risk in ~20,000 schools in England. In doing so, we demonstrate an approach for bringing together the advantages of open-source spatial risk assessment frameworks, data science techniques, and physics-based building models to assess climate risk in a spatially consistent way, allowing for the prioritisation of adaptation action in this vulnerable young population. Specifically, we assess the expected number of days each school overheats (internal operative temperature exceeds a high threshold) in a school-year based on three global warming levels (recent past, 2 °C and 4 °C warmer than pre-industrial). Our results indicate an increase in this risk in future warmer climates, with the relative frequency of overheating at internal temperatures in excess of 35 °C increasing more than at 26 °C. Indeed, this novel demonstration of the approach indicates that the most at-risk schools could experience up to 15 school days of internal temperature in excess of 35 °C in an average year if the climate warms to 2 °C above pre-industrial. Finally, we demonstrate how the spatial consistency in the output risk could enable the prioritisation of high risk schools for adaptation action.

* Corresponding author.
E-mail address: laura.dawkins@metoffice.gov.uk (L.C. Dawkins).

https://doi.org/10.1016/j.crm.2024.100602
Received 6 October 2023; Received in revised form 9 March 2024; Accepted 10 March 2024
Available online 13 March 2024

1. Introduction

Climate change is already having an effect on the world, bringing more regular drought, rising sea levels and causing changes in rainfall patterns (IPCC, 2022). Further, high temperatures are increasingly affecting health and well-being (Betts and Brown, 2021). For example, the 2018 and 2020 heatwaves caused approximately 2,500 excess deaths in the UK in each year Thompson et al. (2022), and the 2003 heatwave caused 70,000 deaths across Europe and 2,000 in the UK Johnson et al. (2005). More recently, in July 2022, the UK experienced an unprecedented extreme heatwave, with temperatures reaching 40.3 °C in Coningsby (Lincolnshire), and exceeding 37 °C in large parts of England. As a result, widespread health impacts were experienced in care settings (including hospitals, care homes and schools), public transport was severely disrupted due to failed infrastructure, and a record number of wildfires were experienced, destroying habitats and impacting air quality. Subsequently, the summer of 2022 resulted in the highest heat mortality in the UK since the introduction of the Heatwave Plan for England in 2004, with 2,985 excess deaths (UK Health Security Agency, 2022). In future years, these conditions are projected to increase in frequency and severity with climate change (Hanlon et al., 2021; Arnell et al., 2021), meaning the related impacts will become increasingly common both in the UK and throughout the world.

For individuals, organisations, and governments to make informed decisions about how to adapt to climate change, it is important to not only quantify how the meteorological conditions (the hazard) may change, but how this translates into a change in risk. That is, the impact these future extreme weather events might have on the exposed people, assets and/or ecosystems. Specifically, following the Intergovernmental Panel on Climate Change (IPCC) definition, risk is often assessed by combining information about the hazard (e.g. temperature), exposure (e.g. the location of schools) and vulnerability (e.g. the thermal response of the school building) to compute metrics necessary for assessing risk (e.g. the expected number of times the building will overheat in a year).

Further, it is particularly important to understand the risk associated with the most vulnerable populations and/or infrastructures, so those most at risk can be prioritised for adaptation action. In particular, children may be considered to be a more vulnerable population group due to their lower self-awareness of the effects of overheating and the measures required to reduce this risk (e.g. drinking enough water and staying out of the sun), requiring intervention from adults/teachers (UK Health and Security Agency, 2023). This motivates the need to quantify overheating risk in schools, and also identify which schools are at most risk and must be prioritised for adaptation.

In the UK, similar to many other countries, there is a requirement for the government to undertake a Climate Change Risk Assessment (CCRA) every 5 years, to assess risk, understand adaptation priorities and measure progress in adapting to reduce climate risk. The third UK CCRA (CCRA3) was published in 2022. This highlighted the limited progress that had been made in addressing the increasing risks from overheating in UK houses, health and care facilities, schools, and prisons, many of which are occupied by the most vulnerable groups within the population. In addition, it was hypothesised that policies to address Net Zero, such as introducing high levels of insulation in new and existing homes to increase energy efficiency, may increase the risk of overheating, emphasising the need to tackle the full range of building interventions in a holistic manner (Kovats and Brisley, 2021).

Following CCRA3, the third UK National Adaptation Programme (NAP3) was published in July 2023 (DEFRA, 2023), setting out the actions that government will take to adapt to the impacts of climate change over the period 2023–2028. As part of this programme, government departments (including the Department for Education) have committed to undertaking further research to better understand climate risk, and to taking adaptation action to reduce this risk, prioritising those locations most at risk. Within the education sector specifically, DfE (the Department for Education) have recognised the 'significant threat' of rising overheating in the school stock, and highlighted the need for further research to better understand this risk (DFE, 2023). A recent report by the CIBSE School Design Group in conjunction with industry-wide experts, developed a range of 'good practice' recommendations for adapting school buildings to a warming future (Taylor, 2021). These focused on passive design measures mostly, including the reduction or removal of excess heat, upgrading windows and shading elements, and passive cooling through the use of exposed thermal mass. Another recent report, focussed on adaptation strategies for London schools, echoed many of these suggestions (Mayor of London, 2020). Alongside discussion of measures such as solar shading, improved insulation, alongside Building Management Systems (BMS), the report outlined potential practical applications, and proposed potential frameworks for funding these measures. Several recent papers have also explored the risks of overheating within the English school stock through modelling (Grassie et al., 2023); (Dong et al., 2023b). Outside of the education sector, recent studies have also explored overheating in sectors such as domestic homes (Arup, 2022); (DLUHC, 2019) and care homes (Tsoulou et al., 2022). In line with the aforementioned guidance for schools, passive adaptation approaches were explored by Oikonomou et al. (2020) in their examination of climate change adaptation measures in London care homes.

These studies estimate building conditions and performance, and explore potential refurbishment interventions using physics based calculations and simulations from advanced building models (Dong et al., 2023b). These analyses provide a detailed representation of the vulnerability of different buildings to overheating, based on, for example, their construction type, ventilation system and occupant activities, and provide a 'digital twin' of the building which can be used to assess the relative benefits of different building modifications.

These studies are, however, largely based on a limited representation of the hazard, predominantly simulated using the Chartered Institution of Building Services Engineers (CIBSE) weather files (Mylona, 2012). These weather files provide a valuable tool for building modelling as they contain multiple meteorological variables on a high temporal resolution (hourly), representative of a selection of future climate scenarios, in a format that is easily ingested into relevant software, such as EnergyPlus (US Department of Energy (2021)). Their limitation is in their representation of the spatial variability of the meteorological variables, as they provide just one time series of weather data to represent all locations within a given region, taken from a representative 'regional location' (e.g., Heathrow Airport is used to represent all locations in the Thames Valley region of the UK). If such data is used to assess risk at multiple locations, this is equivalent to assuming the climate hazard is fully dependent throughout each region (i.e., the same temperature is

experienced by all locations in that region at the same time).

In doing so, the influence of local geography (e.g., the altitude or urbanisation) and the resulting local variability in the hazard (e.g. temperature) is not captured. This means that risk estimated across multiple locations will not realistically represent how the hazard (and hence the risk) varies across space during a given event, and in general, leading to under- and overestimation of location specific risk (see Section 3.1 for a demonstration of this). Further, any change in the spatial structure of the hazard (e.g. heatwaves becoming larger in spatial scale due to climate change) is not fully captured. This is particularly important when quantifying and comparing risk across geographically distributed infrastructure and assets (e.g. to prioritise adaptation action), as well as when assessing risks associated with a cascade through a system, where the impact felt at a given location is also dependent on how the hazard impacts other locations (e.g., in a supply chain).

Similarly, until recently a non-spatially coherent approach has been taken in flood risk assessment in the UK. Specifically, a 'local-dependence framework' approach underpins the National Flood Risk Assessment in England (Environment Agency, 2009) and the flood projections within CCRA3. As explained by Sayers et al. (2023), this approach assumes that the probability of the flood hazard is fully dependent across the area of interest. That is, a floodplain is assumed to experience the same severity of flood event (e.g. 100-year return period in-river water level) at the same time. They describe how this assumption may be reasonable at a very local scale, but becomes increasingly in error at larger scales. Sayers et al. (2023) compare flood risk estimation using this local-dependence framework and using a fully spatially coherent event-based framework, and show how the local-dependence approach underestimates future expected annual damages from fluvial flood risk by a factor of approximately 1.5. This highlights the importance of using spatially coherent hazard data in risk assessments. Similarly, the UK Climate Change Committee (CCC) have highlighted the need for more advanced representation of the spatial variability of risk in the next CCRA – CCRA4.

While currently underutilised, the benefits of spatially coherent climate risk assessments have been demonstrated in the literature for a number of use cases. For example, (Hawchar et al., 2020) developed a GIS-based method to understand the geospatial impacts of climate change on critical infrastructure across Ireland. The ability to gain a spatially coherent view of the changing climate hazard enabled'risk hotspots' to be identified, adding value to regional and local risk assessments. Similar work was carried out by (Crespi et al., 2023) to inform the Climate Impact and Risk Assessment for Germany. Here, the ability to identify risk hotspots was used to prioritise action and identify adequate adaptation measures.

Another approach for assessing climate risk in a spatially coherent way is to apply a spatial climate risk assessment framework. Similar to catastrophe modelling in the insurance sector (Clark, 2002), these frameworks combine spatially coherent information about the hazard, exposure and vulnerability to assess risk, capturing all relevant locations in space coherently together. As described by Dawkins et al. (2023a), in recent years, open-source platforms have been made available, allowing for greater flexibility in the quantification of spatial risk, specifically enabling their application to non-financial risk quantification. Examples include CLIMADA (Aznar-Siguan and Bresch, 2019) and RiskScape (Paulik et al., 2022), and these have been used in many regions to assess a range of risks in a spatially coherent way. For example, Stalhandske et al. (2022) use CLIMADA to spatially coherently quantify future heat related risk in terms of mortality and labour productivity across Switzerland, Lan et al. (2023) use RiskScape to assess the indirect impacts of extreme sea level flooding on critical infrastructure (e.g. electricity, water and telecommunications) at different locations in a region of New Zealand (enabled by the spatial coherence of the modelling), and Dawkins et al. (2023a) use CLIMADA to assess the risk to labour productivity due to extreme heat and humidity, spatially coherently across the UK.

Here, we present an application of the CLIMADA based spatial climate risk assessment framework developed by Dawkins et al. (2023a), to assess overheating risk in approximately 20,000 schools in England, to help inform government risk planning for the vulnerable young population. This study combines the benefit of a spatially coherent risk assessment (by applying the CLIMADA based framework) with the benefits of using a detailed building simulation model (as has been developed for schools by Grassie et al., 2023). This is achieved by using the relationship between outdoor and indoor thermal conditions from the building model simulations to inform the characterisation of the physical vulnerability component of the risk assessment for each school. In this study, overheating risk is quantified as the number of times internal operative temperature exceeds a high threshold. The impact of temperature on 'loss of learning' is also a key risk metric of interest to the education sector. This is not included here, but is a plausible extension of the analysis as the number of pupils in each school is known, and the relationship between temperature and cognitive performance has been studied (e.g. Dong et al., 2023a). Finally, the Dawkins et al. (2023a) extension of the CLIMADA platform retains and provides a richer quantification of climate model ensemble uncertainty by using a statistical technique to model and stochastically simulate alternative realisations of climate risk (described in more detail in Sections 2.1 and 2.8). Throughout, we provide a comparison of the results from this spatially consistent risk assessment with those produced using hazard (temperature) information from one location to represent all locations within a given region (i.e. the equivalent non-spatially coherent regional approach described above).

As a result, this study provides a potential blueprint for other organisations (e.g. government and industry) aiming to assess the future climate risk of overheating in buildings in a spatially coherent way, allowing for the comparison and prioritisation of spatially distributed assets. In the case of the UK government, this could provide insight to inform transparent and robust adaptation decision making as part of NAP3, and spatial risk assessments in CCRA4.

Section 2 presents the material and methods developed and applied in this study, Section 3 presents and discusses the results, a consideration of the limitations of the study is included in Section 4 and the implications for risk management are discussed in Section 5.

2. Material and methods

2.1. Assessing climate risk

This study provides an alternative application of the spatial risk assessment framework developed by Dawkins et al. (2023a) and used within Dawkins et al. (2023b) (see both references for more detail). The climate risk assessment and statistical modelling steps within this framework are presented in Fig. 1.

Consistent with the IPCC definition of risk, this framework combines information about the hazard (e.g. temperature), exposure (e.g. the location of schools) and vulnerability (e.g. the thermal response of the school building) to compute metrics necessary for assessing risk (e.g. the expected number of times the building will overheat in a year). Specifically, the framework combines spatially consistent representations of these input factors, i.e. capturing all relevant locations in space coherently together, and varying realistically in space. This allows for the impact of a given extreme event to be compared across space, and for the prioritisation of individual assets based on risk. The hazard maps are a spatially consistent representation of weather events described in terms of their physical intensity/magnitude, and their probability of occurrence (i.e. frequency). The exposure maps provide spatially consistent information about the assets of interest (e.g., people/infrastructure/eco-systems) including their spatial location and characteristics (e.g., building age and type). The vulnerability function represents the sensitivity of the exposed assets to the hazard, and can vary for each asset of interest.

Initially, the climate risk modeller must make a number of choices about the way in which these input factors are represented. Here, these choices are represented by five categories: the hazard data calibration method; the source of the hazard data; the global warming level of interest (e.g., 2 °C above pre-industrial); where the exposed asset information is taken from; and how the vulnerability function (s) are represented/parametrised. In Dawkins et al. (2023b) these subjective modelling choices are varied to explore the uncertainty and sensitivity of risk. Here, a single set of choices are used, described in more detail in Sections 2.2–2.6. An important extension of the analysis presented here could explore the uncertainty and sensitivity of risk to variations in these choices. This could help inform the robustness of the resulting risk quantification, and ultimately the robustness of adaptation actions that could be taken to reduce risk.

Once these input factors have been specified, the 'risk modelling chain' is carried out (see Fig. 1). The first step in this chain applies the open-source probabilistic event-based risk assessment platform, CLIMADA (Aznar-Siguan and Bresch, 2019), to estimate risk. Since

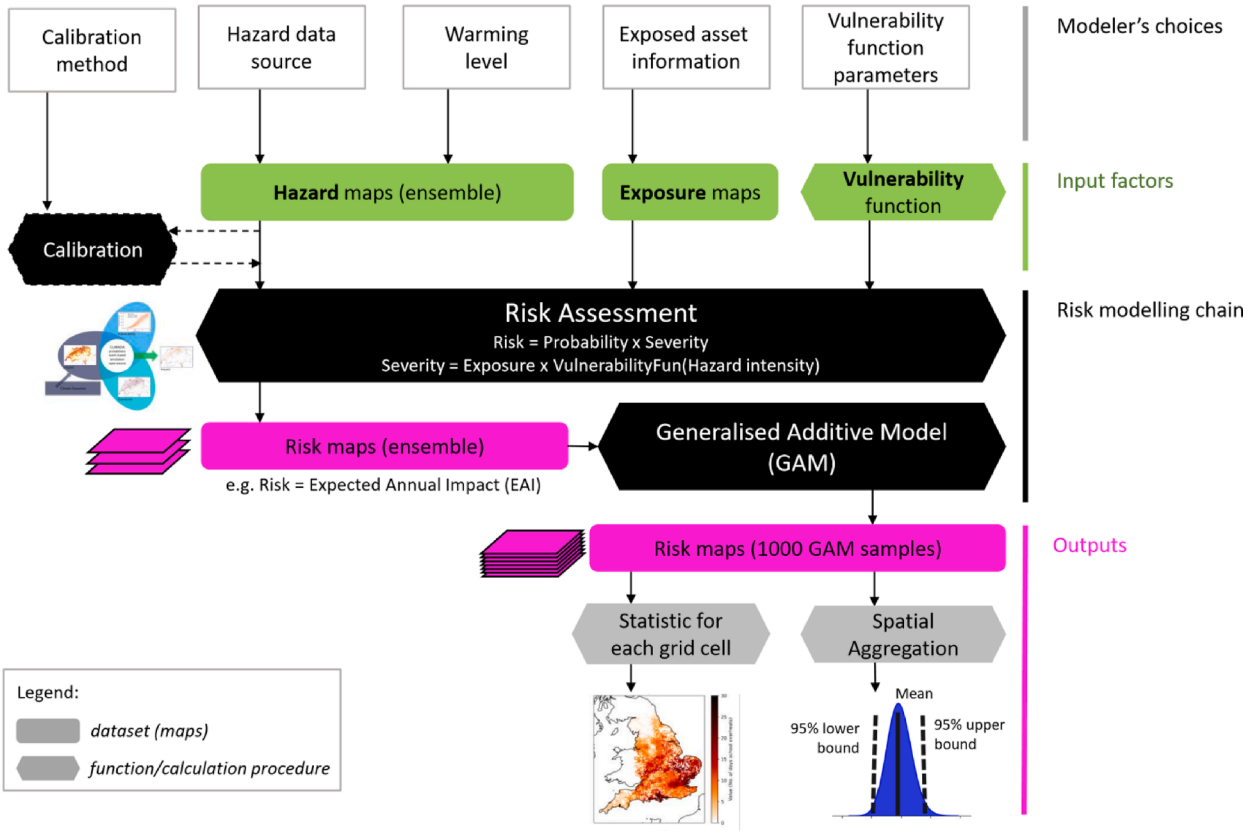

Fig. 1. A schematic demonstrating the climate risk assessment modelling chain, the modeller's choices associated with the model input factors, and the resulting outputs explored in this study. Each part of this framework is described in more detail in the following sections, with an overview given in this section.

the input factors are provided in a spatially consistent way the resulting risk calculation is also spatially consistent. The risk at a given location is estimated as:

$$\text{Risk} = \text{Probability} \times \text{Severity} \tag{1}$$

$$\text{Severity} = \text{Exposure} \times f_{vuln}(\text{Hazard Intensity}), \tag{2}$$

where f_{vuln} is the vulnerability function. The definition of 'Probability' used in this study is described in Section 2.7.

As described in Dawkins et al. (2023a), within the framework presented here, the hazard maps used within the CLIMADA platform are taken from climate model projections. Climate projections often comprise a number of ensemble members, which are alternative realisation of the modelled period produced to capture the uncertainty associated with internal variability of the climate system (aleatoric uncertainty). Here, the risk assessment is applied to hazard maps of weather events taken from each available ensemble member separately, resulting in an ensemble of risk maps, characterising the risk based on each ensemble member.

Climate models are very computationally expensive to run, hence there is often a limit to the number of ensemble members that can be produced. This subsequently limits quantification of uncertainty across these ensemble members, particularly for extreme events. To help to overcome this, the next step within the 'risk modelling chain' (Fig. 1) uses a Generalised Additive Model (GAM) to statistically model risk across space, representing the distribution of ensemble members together, while taking into account the differences between them. This statistical model is then used to sample many more realisations of risk, representative of a larger collection of plausible ensemble members, providing a richer quantification of the aleatoric uncertainty in risk. See Dawkins et al. (2023a) for more detail, and Section 2.8 for a description of the GAM implemented in this application of the framework.

The subsequent output of the end-to-end framework is a representation of the probabilistic predictive distribution of risk (spatially coherently at each location in the region). In practice, this is quantified using 1000 samples of risk from the fitted GAM. These samples can be used to represent the full predictive distribution of risk or quantify any statistic of it, such as the mean or the 95 % prediction interval (i.e. the uncertainty in the predicted risk). In addition, the risk can be considered for each location or aggregated over space to represent a given region, as shown in Fig. 1.

The next sections describe in more detail the modelling choices made to represent hazard, exposure and vulnerability within this study, subsequently used to assess overheating risk in ~20,000 schools in England.

2.2. Hazard: Data source

In this study, the physical intensity of the hazard is defined as the outdoor daily mean air temperature near the Earth's surface (2 m above). This hazard variable is translated into indoor daily maximum operative temperature and subsequently overheating severity via the vulnerability function (see Section 2.6). Similar to Dawkins et al. (2023a) and Strauss et al. (2021), each day in the data record used is considered to be a hazard 'event', and the frequency of each event is then calculated based on the the number of days in the overall event set used. Further, to ensure school-year relevant temperature information and event frequencies, the month of August is removed (as this coincides with the UK summer school holidays), and each school year is assumed to consist of 195 days (to take into account weekends and other school holidays).

In order to represent the spatial variability in the hazard, as well as past and future climate, in this study and similar to Dawkins et al. (2023a), the hazard information is taken from the UK Climate Projections 2018 (UKCP18 Murphy et al., 2019). UKCP18 includes a 12-member Perturbed Parameter Ensemble (PPE) from a 12 km resolution regional European model (Lowe et al., 2018). These projections are forced at the boundaries of the European domain by a corresponding PPE of the HadGEM3 global climate model (Williams et al., 2017). Since these 12 RCM simulations are driven only by the Hadley Centre global climate model (GCM), they only sample a subset of the plausible climate uncertainty range. Using a global warming level approach for defining future periods of interest (see Section 2.4) partially reduces this problem. To enhance the representation of climate model uncertainty additional sources of climate information could be included within the study, as in Dawkins et al. (2023b). This is beyond the scope of this study but would be a relevant extension for future work. In addition, future work could look to implement the recently updated convection-permitting model (CPM) high resolution (2.2 km) projections from UKCP18 (MOHC, 2019).

The UKCP18 RCM ensemble uses the Representative Concentration Pathway (RCP) 8.5 scenario, and provides simulated data for the period 1981–2080 on a daily temporal resolution. The RCP8.5 scenario is a high emissions scenario, and hence may lead to greater warming than will occur based on current global climate policies (i.e. implying a back tracking on current policy pledges). However, using this RCP enables consideration of a wide range of global temperature increases within the 21st century (Riahi et al., 2011), allowing for both 2 °C and 4 °C global temperature increases (above the pre-industrial level) to be considered, as recommended in the most recent UK Climate Change Risk Assessment (CCRA3, Betts et al., 2021).

2.3. Hazard: Calibration method

As discussed by Garry et al. (2021), biases exist within the UKCP18 RCM temperature data. As such, similar to Garry et al. (2021) and Dawkins et al. (2023a) we apply bias correction to the data, using the the Scaled Distribution Mapping (SDM) approach of Switanek et al. (2017). While calibration can only go so far in addressing model limitations (Thompson and Smith, 2019), Garry et al. (2021) showed an improvement in the UKCP18 representation of temperature data relative to observations when using this approach. This bias correction is applied to daily mean temperature separately for each climate model ensemble member, each variable and each grid cell in the UK, using HadUK-Grid (Hollis et al., 2019) to represent historical observations. Each calendar month is bias corrected

separately, using the historical base period 1998–2017. This bias correction is applied to 21 year rolling windows, retaining only the central year of each 21 year block (to ensure continuity in the corrected data). As such, for the UKCP18 RCM projections (which are available to 2080) data beyond 2070 cannot be bias corrected with a 21-year window and is hence omitted from the study.

2.4. Hazard: Warming level

Akin to previous applications of this framework (Dawkins et al., 2023a,b), and consistent with CCRA3 guidance (Betts et al., 2021), three global warming levels are considered here: current/recent past, and 2 °C and 4 °C increase in global mean temperature beyond the pre-industrial level. These warming levels align with two policy relevant future pathways (1) stabilising at 2 °C warming by the end of the century (2100), representing achievement of the goals set out by the Paris Agreement, and (2) 4 °C global warming by the end of the century, consistent with the trajectory expected to occur based on the limited global ambition for reducing emissions as of the date of publication of CCRA3.

Similar to many examples (Garry et al., 2021; Hanlon et al., 2021; Nikulin et al., 2018; Schleussner et al., 2016; Iturbide, et al., 2021), a time slice approach is used here to identify periods that represent each warming level. Specifically, we follow the IPCC approach (rather than the end of century CCRA3 approach) which allows for the time window of the warming level to be reached at any point within the data record time period.

Consistent with Garry et al. (2021), Dawkins et al. (2023a) and Dawkins et al. (2023b), the current climate (recent history) is represented by the period 1998–2017. For the 2 °C and 4 °C above pre-industrial warming levels, a similar approach to that used in the Intergovernment Panel on Climate Change (IPCC) interactive atlas is used (Nikulin et al., 2018). For each of the 12 UKCP18 RCM ensemble members, the year in which the level of mean global warming (i.e., 2 °C and 4 °C) is reached in the associated global driving simulation is found from a moving 21-year mean of global temperature anomaly. This year is then used as the central estimate for defining the future period (9 years prior and 10 years post). Here, as in Dawkins et al. (2023a), the central years are taken from the analysis of Hanlon et al. (2021). In cases where less than 15 years of data are available to represent a given warming level, that ensemble member is not included in the analysis. Here, this means UKCP18 RCM ensemble members 08, 10 and 15 are omitted from the analysis for the 4 °C warming level.

2.5. Exposure: Location and characteristics of schools

The exposed asset information used within this study consists of the graphical location of each of the 19,158 schools included in the analysis (of the ~22,000 state schools in England). These locations are shown in Fig. 2 (a) and (b). This representation of the graphical location of schools allows for the hazard intensity, taken from the spatially consistent gridded UKCP18 projections, to be mapped to the location of the exposed assets within the risk assessment.

In addition, a number of characteristics of each school are captured and used to identify the relevant vulnerability function to use

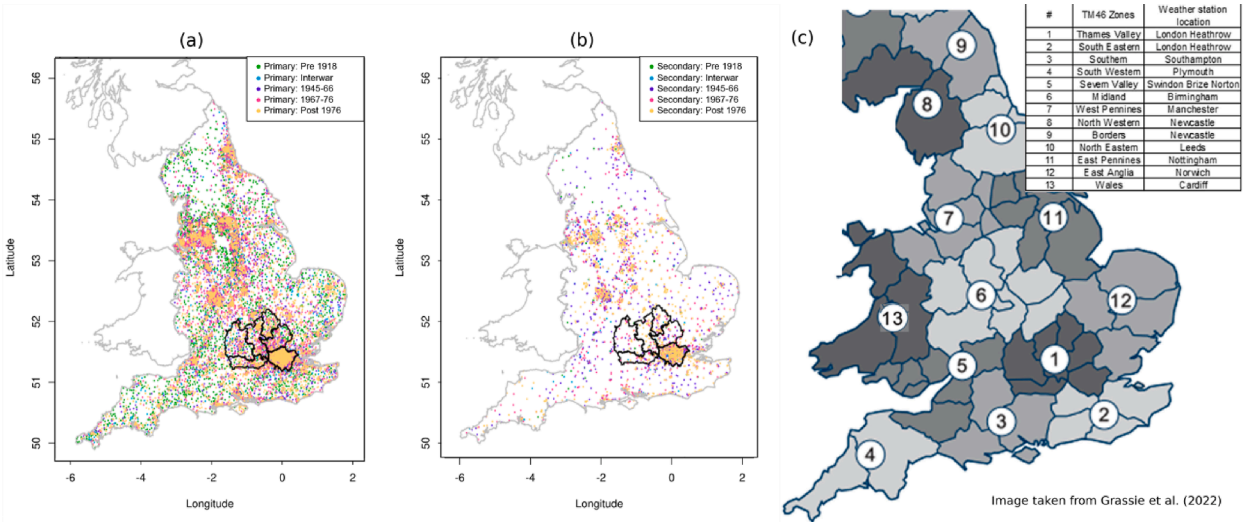

Fig. 2. A graphical representation of the exposure information used within this study, including (a) and (b) the geographical location of the 19,158 schools included in the study, shown for primary and secondary schools respectively, and school characteristic information required for mapping each school to a vulnerability function: in (a) and (b) the education phase and building era of the schools, and (c) the 13 geographical regions schools are allocated to (taken from Grassie et al. (2023), based on a figure from CIBSE (2008)). In this study, the vulnerability functions are developed using building stock simulations from Grassie et al. (2023), where simulations from each stock model are based on regional weather files. The locations of the regional weather files used for this are also given in (c). See Section 2.6 and Grassie et al. (2023) for more detail. The components of the Thames Valley region have been outlined on panels (a) and (b) for reference as this area will be used as a illustrative example later in this study.

for that school within the risk assessment (see Section 2.6). These include which of the CIBSE geographical regions the school is located in (see Fig. 2 c); the era/period in which the school was built and the associated building fabric thermal properties; and the education phase of the school, which drives the activities within the schools, and the associated level of heat that is generated through these activities (see Table 1). It should be noted that each school is represented as one building/classroom, and hence the existence of different school buildings and floors within buildings is not captured here.

The 19,158 schools included in this study are all of the open primary and secondary schools in England (as of November 2022) for which information about all of these required school building characteristics is available. This information is taken from the Department for Education's Property Data Survey Programme (PDSP) survey of the school building stock (Education & Skills Funding Agency, 2016), in conjunction with their 'Get Information About Schools' database (Department for Education, 2017).

Since the study focuses on the risk of each school overheating, other metrics such as the monetary value of the building or the number of pupils/occupants, are not considered. Relevant future work could look to extend this to assess the overheating risk weighted by the number of occupants to highlight those schools more at risk due to the greater number of pupils exposed. Indeed, as previously noted, loss of learning is a key risk metric of interest to the education sector, and hence in this case the number of pupils in each school will be important to include. Further, the assessment of alternative risks such as flooding are likely to require information on the monetary value of the school building.

2.6. *Vulnerability: Relating outdoor temperature to indoor overheating in schools*

The aim of the vulnerability function is to characterise the relationship between the intensity of the hazard (e.g. temperature) and the impact of interest (e.g. overheating in a school). Here, this means developing a function that characterises the relationship between outdoor daily mean temperature (the hazard information taken from the climate projections, see Section 2.2) and whether an indoor 'overheating' temperature threshold is exceeded (to allow for the assessment of overheating frequency). This necessitates first the quantification of the relationship between outdoor daily mean temperature and indoor daily maximum temperature, where this relationship will vary between schools depending on the characteristics of the school/classroom (e.g. construction age and orientation).

There are a number of potential ways to quantify the relationship between outdoor and indoor temperature. For example, one could collect relevant temperature data using sensors placed inside and outside of representative buildings. Alternatively, there is a growing body of literature in the use of building stock modelling to assess indoor building thermal conditions (Grassie et al., 2022; Dong et al., 2023b; Grassie et al., 2023; Schwartz et al., 2022). Specifically, here we quantify the relationship between outdoor and indoor temperature using insights from a specific building stock modelling approach known as a bottom-up engineering approach. This approach uses building physics to estimate the performance of a building (including internal temperatures as well as energy consumption), based on information about its physical form, internal systems, and occupancy characteristics.

These models generally follow one of two approaches, archetype-based or building-by-building. In the archetype-based approach

Table 1
Categories the building model archetype characteristics (Region, Era and Education Phase) can take within this study. Vulnerability functions are derived for each combination of these three characteristics (130 possible archetypes), and each of the 19,158 schools included in the study are assigned to one of these combinations (e.g. North West, Pre-1918, Secondary).

Category	Options
Region	Thames Valley
	South East
	Southern
	South West
	Severn Valley
	Midlands
	West Pennines
	North West
	Borders
	North East
	East Pennines
	East Anglia
	Wales
Era	Pre-1918
	1918–1945
	1945–1967
	1967–1976
	Post-1976
Education Phase	Primary
	Secondary

each modelled building is categorised as one of a number of representative building 'types' based on characteristics such as age. This allows for the whole building stock to be represented by a reduced number of representative models, reducing the required computational resource. The limitation of this is that the archetypes are unlikely to capture the heterogeneous characteristics of each building. Conversely, building-by-building approaches aim to create models for every individual building, taking into account the differences in their individual features. As a result the computational complexity and data requirements are larger but the detail of the modelling is enhanced.

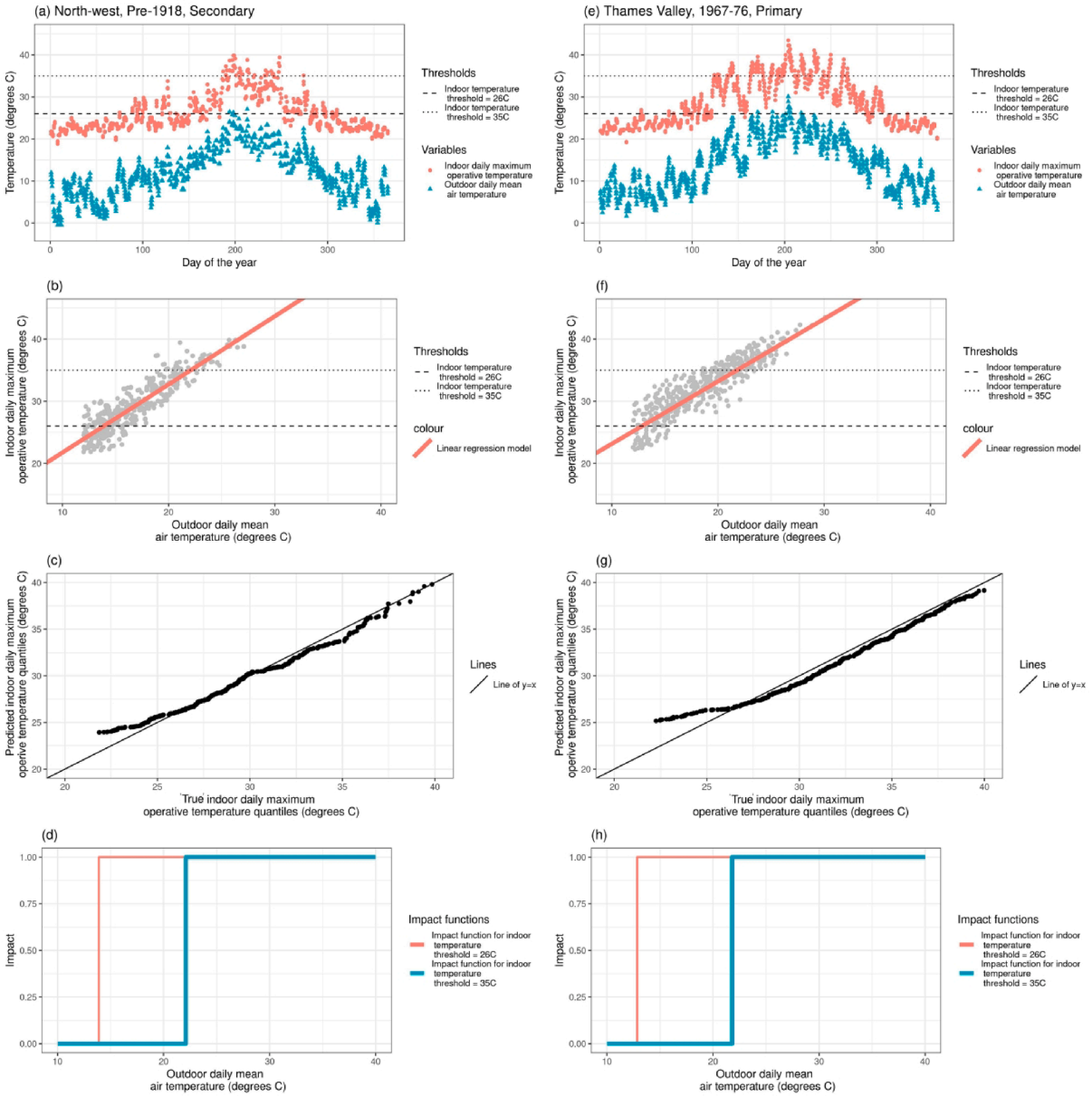

Fig. 3. A demonstration of the construction and validation of vulnerability functions for two school building archetypes (left column) North-west, pre-1918, secondary, and (right column) Thames Valley, 1967–1976, primary. Plots (a) and (e) show time-series (based on'day of the year') for indoor (south facing classroom) and outdoor temperature variables (for days when the classroom is occupied) for the three design summer year climate scenarios used in the building model simulations. Horizontal dashed lines are included to show the two indoor overheating temperature thresholds considered in this study. Plots (b) and (f) show the same temperature variables as scatter plots (truncating above central heating level) and the best fit linear model fitted to these points to predict indoor daily maximum operative temperature from outdoor daily mean temperature. Plots (c) and (g) show Quantile-Quantile plots as validation of the fitted linear models, quantifying the agreement between the 'true' (i.e. from the building simulations) and predicted (i.e. from the linear model) quantiles of indoor daily maximum operative temperature. Plots (d) and (h) show the two final vulnerability step functions that translate the hazard (outdoor daily mean temperature) to impact, i.e. whether or not the indoor overheating threshold (26 °C or 35 °C) is exceeded in the south facing classroom.

Primarily, building stock models have been used to explore energy efficiency in buildings to aid in understanding strategies to reach net-zero policy targets (Godoy-Shimizu et al., 2022). More recently, however, these models have been implemented to explore overheating risk, including in school classrooms as in the archetype based approach of Grassie et al. (2023). We use a subset of the model simulations from Grassie et al. (2023) within this study to quantify the relationship between outdoor daily mean temperature and indoor daily maximum temperature in UK schools (processed from the simulated hourly temperature profiles). Work is currently ongoing to extend this to the use of a more detailed building-by-building approach.

Grassie et al. (2023) implement a bottom-up engineering archetype-based approach to assess environmental conditions, including overheating, for future energy retrofit scenarios across the UK school building stock. The building stock models of Grassie et al. (2023) are derived from a single EnergyPlus seed model (US Department of Energy (2021)), incorporate four different classroom orientations (North-South-East-West) to allow for the assessment of the sun's orientation impact, and include 195 archetype descriptions and a number of retrofit and climate scenarios. The simulations are carried out on a classroom-level (rather than a whole school level) to allow for the assessment of overheating in a confined learning environment. The archetype descriptions are characterised by thermal-related characteristics (1) phase of education (primary or secondary), (2) construction eras (e.g. pre-1918) and their associated construction build-up, (3) graphical region (e.g. Thames Valley), and (4) ventilation type (natural or mechanical). Each of the schools considered in the study (see Fig. 2) can then be allocated to one of these archetypes, based on their characteristics. As a relatively small proportion of schools have mechanical ventilation and in some cases the ventilation type information is missing, for simplicity here we consider all schools to have natural ventilation and use building simulations from archetypes with natural ventilation only. The 19,158 schools include within this study are therefore allocated to an archetype based on characteristics (1)-(3) only (e.g. as described in Section 2.5). The categories these archetype characteristics can take are shown in Table 1. Further, here we do not consider any retrofit scenarios and focus solely on the'base operation' scenario of Grassie et al. (2023).

For each of the 130 archetype combinations shown in Table 1, Grassie et al. (2023) simulate from the relevant stock model using three climate scenarios (2020 s, 2050 s and 2080 s) to represent outdoor meteorological conditions. These are sourced from the CIBSE current and future weather files (Mylona, 2012), which are readily available for use within EnergyPlus. These files represent a 'design summer year' (approximately a 1 in 7 year hot summer) in each of the climate scenarios, with a different file used to represent the meteorological conditions in each of the 13 regions in the archetype definitions (see Fig. 2 c). For the three years of simulations (representative of each decade: 2020s, 2050s and 2080s), these archetype model simulations provide data on (amongst other variables) outdoor daily mean air (dry bulb) temperature (from the CIBSE weather files), the associated hourly indoor *operative* temperature for a classroom at each compass orientation (North-South-East-West), and the hourly people occupant count (from the EnergyPlus models).

Using a regional representation of the weather/hazard is acceptable in this part of the modelling chain because the data is simply being used to quantify the thermal response of the building and is not being used to quantify the overheating risk of the building. We ensure the spatial variability of the hazard is captured within the risk assessment by using the spatially coherent climate projections in the hazard component (Section 2.2).

Indoor *operative* temperature is an alternative temperature variable, based on the air temperature, but with consideration of other factors of the environment such as radiation and convection. As such, the operative temperature can be considered as a measure of the thermal comfort for the occupants of the classroom and is therefore used here to better capture the impact of overheating on occupants.

Time-series of outdoor daily mean air temperature and indoor daily maximum operative temperature (for a south facing classroom) are shown in Fig. 3 (a) and (e), for two of the school archetypes (North-west Pre-1918 secondary schools and Thames Valley 1967–76 primary schools respectively). These include data for the three design summer years used in the simulations. To ensure the indoor daily maximum operative temperature is relevant for occupants of the classroom, this maximum is identified from the building simulation for hours in which the classroom is occupied, information taken from the simulation data of Grassie et al. (2023). The south facing orientation is used here for demonstration as this is likely to be the hottest (exposed to more sunshine in the day). The same analysis could, however, be repeated for other orientations.

The same data and variables are plotted as scatter plots in Fig. 3 (b) and (f) (for indoor temperature greater than 21 °C, on the assumption that this is the temperature maintained by central heating) showing the direct relationship between outdoor daily mean air temperature and indoor daily maximum operative temperature for these example archetypes (i.e. the relationship we want to model). These plots suggest that a linear relationship exists between these variables (a consistent finding across archetypes), and hence that a linear model is most appropriate for capturing this relationship for each archetype (as shown in 3 (b) and (f)):

$$T_{indoor} = a \times T_{outdoor} + b \tag{3}$$

where T_{indoor} is the indoor daily maximum operative temperature, $T_{outdoor}$ is the outdoor daily mean temperature, a is the slope/gradient of the linear model (i.e. the slope of the red lines shown in Fig. 3 (b) and (f)) and b is the intercept (i.e. where the red lines cross the y axis at x = 0 in these figures). Fitting a function of this form for each school archetype allows for T_{indoor} to be estimated from any $T_{outdoor}$, for example taken from future climate projections. More detail on the model fitting, selection, and the resulting linear model parameters for each archetype, are given in the Supplementary Material of this paper.

Fig. 3 (c) and (g) show Quantile-Quantile plots for the linear models for the south facing orientation for these two example archetypes. A model that fits the data well will result in good agreement between the quantiles of the model predictions of T_{indoor} and the 'true' data from the building model simulations (i.e. the points will lie close to the line y = x). These figures show that when indoor daily maximum operative temperature is above 25 °C there is good agreement between the quantiles (hence providing a good fit for the overheating thresholds used: 26 °C and 35 °C). Below this, there is some overestimation in the predicted values. A similar good fit at the

required overheating thresholds is found across the archetypes (not shown).

These models can now be used to construct the final vulnerability functions which relate the outdoor temperature to indoor temperature exceeding a relevant overheating threshold. Here, two overheating thresholds are considered:

1. Indoor operative temperature greater than 26 °C, a threshold considered to be an upper limit of comfortable operative temperature in schools (Table 7-2 in Education & Skills Funding Agency 2018)
2. Indoor operative temperature greater than 35 °C, a threshold considered to have important health impacts on people (Petitti et al., 2016).

The linear regression models (for the south facing classroom orientation) are used to determine the value of $T_{outdoor}$ that relates to T_{indoor} being equal to each of these thresholds for each archetype. When the threshold is exceeded the impact is specified as 1 (i.e. the school overheats). This approach is used to derive vulnerability functions, relating $T_{outdoor}$ (the hazard variable) to impact, for each overheating threshold and archetype, as shown for the example archetypes in Fig. 3 (d) and (h). These functions can therefore be used to relate $T_{outdoor}$ during a given hazard event, taken from gridded spatially coherent climate projections, to the impact felt by a given school (overheating or not). It should be noted that the underlying approach of modelling classroom overheating at a stock level, and validation with monitored data is still undergoing revision. The vulnerability function allows the workings of the physics-based classroom model to be replaced by a statistical function within the climate risk assessment. As the underlying classroom model is revised and validated against monitored data, the vulnerability function must also be updated. To this end, the resulting quantification of risk presented here should not be used in an official capacity for climate risk assessment and/or climate adaptation decision making. Refinements of the method are required to allow for this.

2.7. Risk metric

As described in Section 2.1, within the 'risk modelling chain' part of the spatial risk framework (Fig. 1), the representations of hazard, exposure and vulnerability are combined to estimate the severity of each hazard event at each exposed location. In this case, this severity is either 0 (the school does not overheat) or 1 (the school does overheat). For a given hazard global warming level, the risk is then quantified as some 'probability' of this severity within the related hazard event set.

Here, similar to Dawkins et al. (2023a) and Dawkins et al. (2023b), the risk at each location/school (equation (1) is calculated as the Expected Annual Impact (EAI), i.e. the average annual total severity. Specifically, here this is a quantification of the expected number of days each school overheats within a school year (195 days in a school year with August excluded from the hazard data). Alternative risk metrics, such as the 1 in 10 year event, could be calculated but these are considered by policy makers to be less relevant for climate risk decision making in this school context, where resilience to the expected/average (rather than extreme) conditions is necessary.

2.8. Generalised Additive model for risk

The Generalised Additive Model (GAM) part of the 'risk modelling chain' (Fig. 1) aims to represent risk across the region and climate ensemble members, here summarised as the EAI (see Section 2.7). Once fitted, this statistical model can be used to sample many more realisations of risk, representative of a larger collection of plausible ensemble members, providing a richer quantification of the aleatoric uncertainty in risk. See Dawkins et al. (2023a) for more detail.

This data modelling part of the chain has a set of requirements that need to be met. First, the data integration part where data from each ensemble member are "blended" to an overall estimate. Second, the blending must be performed in a probabilistic way, to enable stochastic simulation of other potential ensemble 'realisations'. Third, the two main sources of uncertainty (1) the estimation of the data blending and 2) the variability of the data about a perceived ensemble mean), need to be quantified and included in the stochastic simulation. As shown in previous work (Dawkins et al., 2023a; Steptoe and Economou, 2023; Economou et al., 2023) GAMs constitute a framework with which all three requirements are satisfied, rendering them, a unique tool suited for the purpose of this work.

More generally, a plethora of machine learning methods have been used in climate and impact risk analysis Zennaro et al. (2021). Unsupervised learning methods such as artificial neural networks and random forests scale well with big data and have good predictive skill at the expense of interpretability. GAMs on the other hand lie somewhere in the middle of the accuracy-tointerpretability spectrum Angelov et al. (2021), the latter part being key in producing robust risk estimates. Interpretability with GAMs also includes probabilistic model checking (given in Section 2 of the Supplementary Material), an often neglected part of validating inference from data models.

Within this application of the spatial risk assessment framework of Dawkins et al. (2023a), the GAM for risk is largely consistent with that applied in Dawkins et al. (2023a) and Dawkins et al. (2023b). Similar to these previous applications, the ensemble of risk maps derived from the climate projection ensemble are modelled as a combination of a smooth function (now of longitude and latitude only) and an ensemble member 'offset' term (to capture the overall mean difference between ensemble members). This ensemble member 'offset' is represented by a stochastic term, known as a random effect (Simpson, 2022), which is able to vary between ensemble members, but is consistent across space. As in Dawkins et al. (2023a), a random effect rather than a fixed effect (i.e. a fixed regression coefficient for each ensemble member to shift the mean up and down) is used to reflect our understanding that the N ensemble members we have available to us are just a sample of members from a larger collection of plausible members which have not been observed/produced (Simpson, 2022). This therefore allows for the prediction of more ensemble member, not just those available

in the climate projection dataset. This means that 1000 simulations from this GAM are equivalent to a statistical estimate of climate projected risk from a climate model ensemble with 1000 members. This increased sample of ensemble members can be thought of as a more comprehensive quantification of aleatoric uncertainty. However, as noted by Dawkins et al. (2023a), simulations from the GAM are limited to representing the particular ensemble being modelled. Hence, if the ensemble is known to structurally miss some of the uncertainty, this will also be the case for the simulations from the statistical model. To overcome this, the statistical model could be applied to ensemble members from many different climate models (beyond the scope of this paper).

In this application, an additional term is included in the GAM to capture the difference in risk between different school building archetypes. This building archetype 'offset' term is represented by a fixed effect which is different for each of the 130 possible archetype combinations (Table 1). This is included as an additive term, accounting for the linear offset in the overheating vulnerability step functions in different archetypes (e.g. as in Fig. 4 d and g). A fixed effect is used here as we specifically want to model the risk associated with the archetypes included in the assessment, rather than simulate alternatives. As in Dawkins et al. (2023a), this model structure is found to be consistent with the structure of the data, identified through exploratory data analysis.

Consistent with Dawkins et al. (2023a), a Gaussian model family is used to describe the logarithm (base 10) of the risk. This family of GAM is used because it allows for both the mean and standard deviation of the risk to vary with the model covariates, which is identified as the appropriate model structure by exploring relationships in the modelled data. Risk is therefore modelled using a Normal (Gaussian) distribution with a spatially varying mean, captured as a smooth function of longitude (lon) and latitude (lat). This allows the risk to vary across space, but ensures a smoothness such that schools of the same archetype that are near to each other have

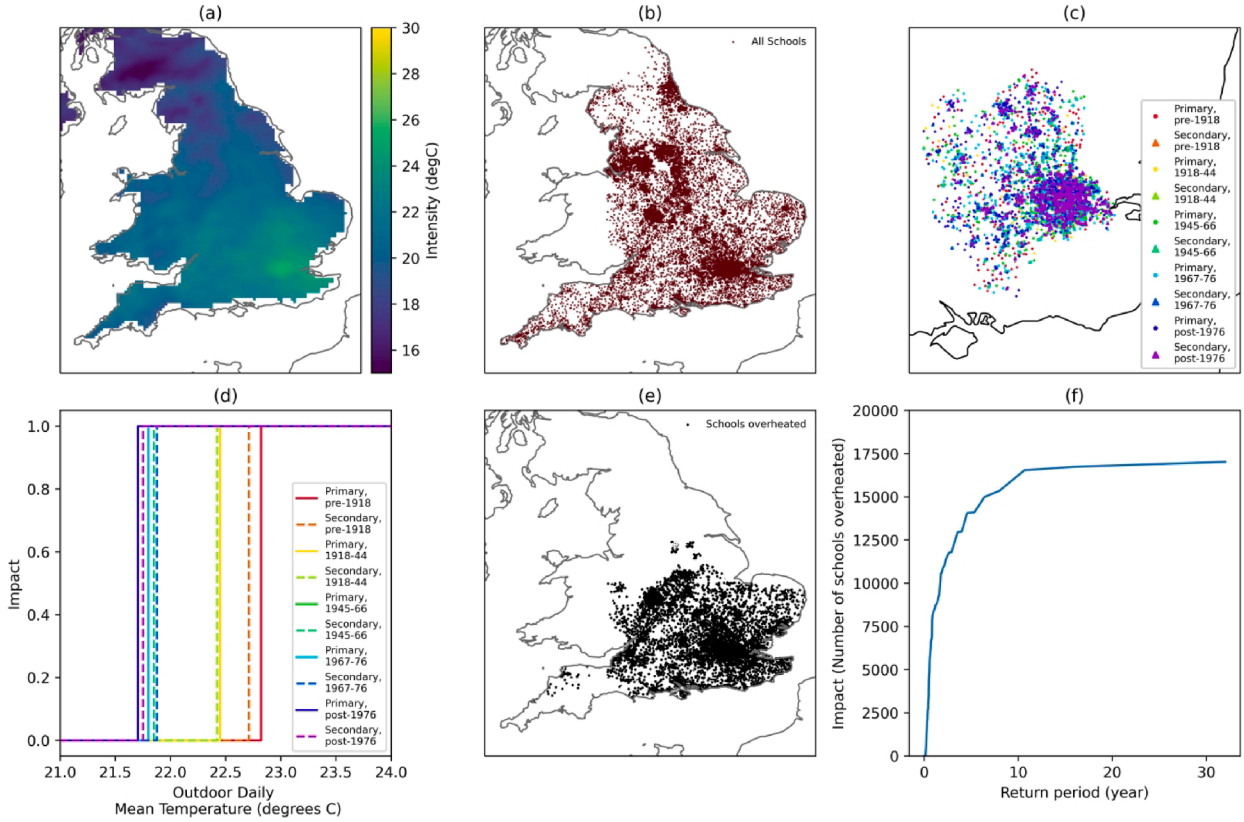

Fig. 4. A demonstration of the hazard, exposure and vulnerability inputs used within the CLIMADA risk assessment platform: (a) Hazard: an example of a hazard event spatial field (daily mean air temperature) from the most extreme day/event (based on UK mean) in the bias corrected UKCP18 ensemble member 01 20 year time slice representing the recent past; (b) Exposure: the geographical location of all 19,158 schools included in the study (of the ~20,000 state schools in England), each of which is given a value of 1 in the exposure component of the risk assessment; (c) Exposure and Vulnerability: a demonstration of the archetypes of schools in the Thames Valley region, input as exposure information and used to relate each school to the relevant archetype vulnerability function; (d) Vulnerability: overheating vulnerability functions representing each school archetype in the Thames Valley region for the 35 °C overheating threshold; (e) Severity: a map of the severity of the hazard event shown in (a) at each school (i.e. overheated or not), for the 35 °C overheating threshold; (f) Severity: exceedence frequency curves for spatially aggregated severity (i.e., number of schools that overheat in each event) for the 20 year time slice representing the recent past taken from UKCP18 ensemble member 01, for the 35 °C overheating threshold. Note: Each school year is considered to be 195 days long, hence each year of data from the 20 year time slice (360 days, with the 30 days of August set to 0 to represent how the school is unoccupied in the summer) represents $360/(195 + 30) = 1.6$ years. The 20 year time slice therefore represents 32 school years, explaining why the exceedence frequency curves are calculated for up to a 32 year return period.

similar risk. This is then combined with the two offset terms described above to capture the differences in risk across ensemble members and school building archetypes. As mentioned above, the standard deviation of risk was also found to vary with covariates (specifically longitude and latitude). Hence in this application (different from Dawkins et al., 2023a), the standard deviation of risk is also modelled as a smooth function of longitude and latitude. That is:

$$\log_{10}(Risk(m,s,a)) \sim N(\mu(m,s,a), \sigma(s)^2), \tag{4}$$

$$\mu(m,s,a) = f(lon(s), lat(s)) + \xi_m + \beta_a, \tag{5}$$

$$\log(\sigma(s)) = f(lon(s), lat(s)), \tag{6}$$

$$\xi_m \sim N(0, \lambda^2), \tag{7}$$

where m represents the ensemble member, s represents the spatial location, a represents the school building archetype and $\log_{10}(\cdot)$ is the log base 10 function which is used to transform risk at each school to the log scale. This transform is performed to ensure risk (the output variable of the model) is symmetrically distributed (as required by the specified GAM model). The GAM then models this log transformed risk using a Normal distribution with a mean, $\mu(m,s,a)$, that varies in space (by long and lat), by ensemble member, and by school building archetype, and standard deviation, $\sigma(s)$, that varies in space (by long and lat). The mean is modelled as a combination of a smooth function of space, $f(lon(s),lat(s))$, (i.e., a spatial regression), a spatially constant ensemble member random effect, ξ_m, and a school building archetype fixed effect, β_a. The ensemble member random effect is in turn modelled using a Normal distribution with zero mean and standard deviation λ.

As in Dawkins et al. (2023a), GAM parameter estimation is carried out using the R package mgcv (Wood et al., 2016) via restricted maximum likelihood estimation (REML), and these parameters estimates are used to simulate alternative realisations of risk from the model to better quantify the uncertainty. Specifically, as described in Dawkins et al. (2023a) and Steptoe and Economou (2021), this can be done in a way that is equivalent to simulating from the Bayesian posterior predictive distribution of the model Gelman et al. (2014). This allows for the full Bayesian posterior predictive distribution to be assessed and Bayesian prediction intervals to be produced for risk at each school. That is, the 95 % prediction interval can be plotted alongside the mean to capture the uncertainty in risk, quantifying the interval the true risk falls within with 95 % probability (according to the model).

3. Results and discussion

This section presents the results of the application of the methods described in the previous section to assess overheating risk in ~20,000 schools in England, for both the current and plausible future climates. In particular, we highlight the differences in using a 'regional location' approach to represent the hazard compared to using a spatially varying hazard field (e.g. taken from gridded climate projections).

3.1. Results: Risk assessment

The CLIMADA open-source climate risk assessment platform is applied to each of the 12 (bias corrected) UKCP18 RCM ensemble members, where 20 year time slices from each member are used to represent the recent past (1998–2017), 2 °C and 4 °C above pre-industrial warming levels (see Section 2.4). Each hazard event is a day within each 20 years and the intensity of each hazard event at each 12 km land grid cell in the UK is characterised by the daily mean air temperature near the earth's surface.

Fig. 4 (a) shows the spatially varying hazard metric (daily mean air temperature) for the most extreme day/event (highest UK average temperature) in the 20 year time slice representing the recent past, taken from the bias corrected UKCP18 ensemble member 01, showing outdoor temperatures of up to 30 °C. The exposure (the location of all schools included in the study) is shown in Fig. 4 (b), and, as a more detailed demonstration of the exposure information, the specific archetypes for the Thames Valley region are shown in Fig. 4 (c), showing the spatial variability in the exposed school building types. Fig. 4 (d) shows the associated Thames Valley archetype vulnerability functions for the 35 °C overheating threshold, developed based on school-building stock model simulations as described in Section 2.6. These show how the hazard intensity (daily mean air temperature) required for overheating varies across different school education phases and building eras within this region. In particular, this highlights how, in this example, pre-1918 schools require the highest outdoor temperatures for overheating to occur (i.e. they remain cooler), while schools built post 1967 overheat at the lowest outdoor temperatures (i.e. are most susceptible to overheating). This is found to be consistent across the regions considered (not shown) and likely reflects differences in typical floor-to-ceiling heights between schools of different construction ages (Grassie et al., 2023).

Within CLIMADA, the hazard intensity at the location of the exposed assets is combined with the exposure relevant vulnerability function to calculate the severity of each event at each exposure (equation (2). The severity of the hazard event in Fig. 4 (a), i.e. the quantification of whether each school overheats or not, is shown in Fig. 4 (e) for all schools, for the 35 °C overheating threshold. These show how during this extreme event a large number of schools in the south of the region experience indoor temperatures in excess of the higher 35 °C overheating threshold. Fig. 4 (f) show the resulting exceedence frequency curve for spatially aggregated severity (i.e., number of schools that overheat in each event, termed the impact) for the full 20 year time slice representing the recent past (taken from UKCP18 ensemble member 01). This curve shows how (for this time period and ensemble member) the impact of overheating is often widespread during individual events/days, impacting a large number of schools at once. For example, Fig. 4 (f) shows how half of

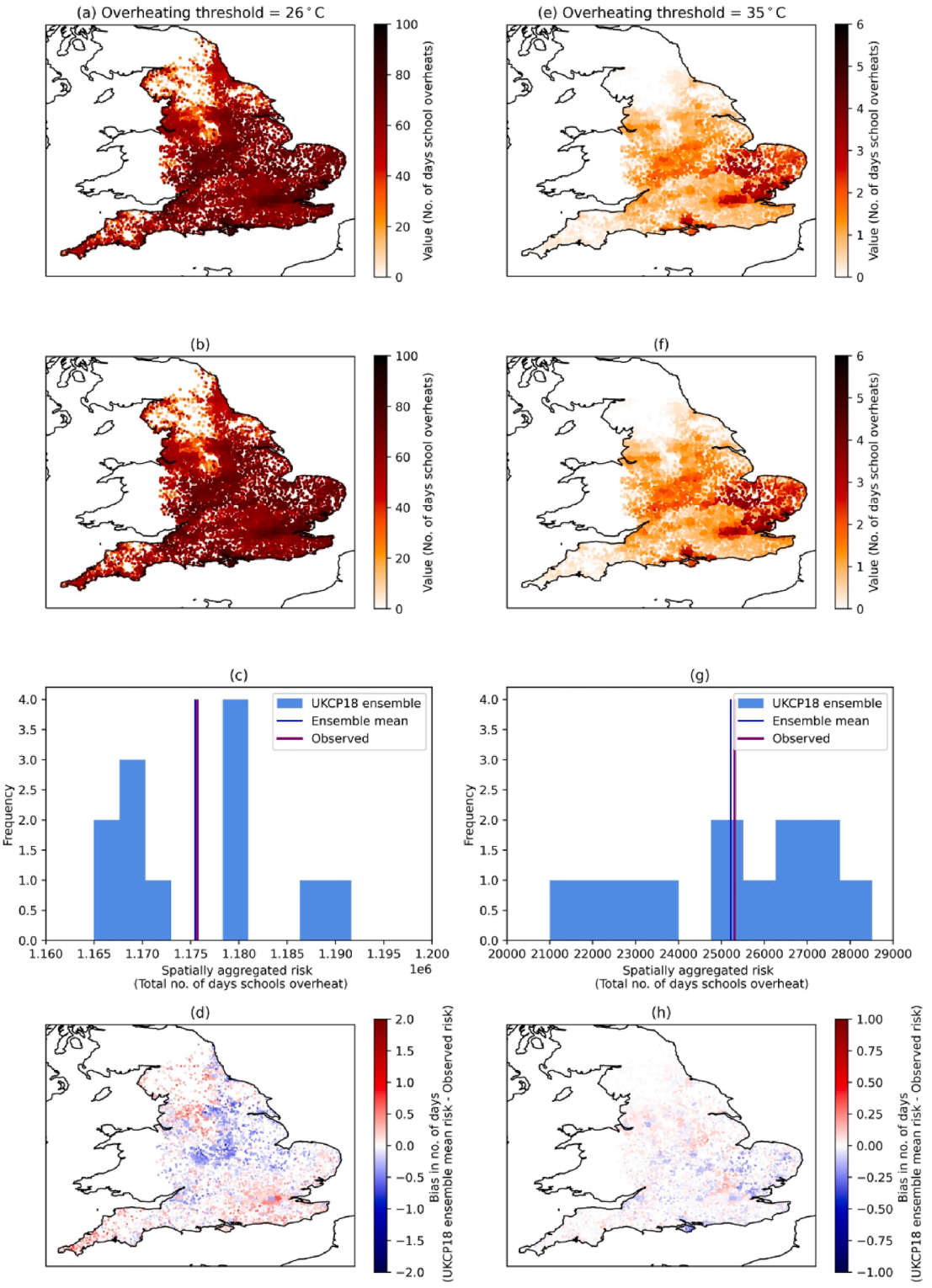

(caption on next page)

Fig. 5. A demonstration and validation of the outputs of the CLIMADA risk assessment platform: (a) the risk (here the expected annual total number of days each school overheats at the 26 °C level) associated with the bias corrected UKCP18 ensemble member 01 time slice representative of the recent historical period (1998–2017); (b) the ensemble mean of risk associated with bias corrected UKCP18 for the recent historical period; (c) a histogram of spatially aggregate risk (summed over schools) from each ensemble member in the recent historical period, with vertical lines representing the ensemble mean, and the equivalent metric calculated using observed hazard data (using HadUK-Grid to represent historical observations for temperature); and (d) the difference between the observed risk and the bias corrected UKCP18 ensemble mean risk for the recent historical period. Positive values indicate that the UKCP18 ensemble mean overestimates risk and vice versa for negative values. Figures (e) - (h) are the same as (a) - (d) but for the 35 °C overheating threshold.

schools simultaneously experience overheating at the 35 °C level approximately once every 2 years. Fig. 4 (f) also shows, however, that (for the recent past and ensemble member 01) there are no events where all schools simultaneously overheat at the 35 °C level.

Building upon Fig. 4, Fig. 5 (a) and (e) show the resulting risk metric (here the expected annual impact, EAI) for the two different overheating thresholds, based on UKCP18 RCM ensemble member 01. The same analysis is repeated for each of the 12 climate model ensemble members, and Fig. 5 (b) and (f) show the ensemble mean of the risk metric. As described in Section 2.2, the month of August is removed the risk calculation (to reflect UK summer school holidays), and each school year is assumed to consist of 195 days (to take into account weekends and other school holidays). As such, the risk estimates shown are specifically focused on the annual impact within the school year (not the calendar year).

Fig. 5 (b) and (f) show how, in the recent past, the risk of overheating is highest in parts of the south and east of England, as well as London. Fig. 5 (c) and (g) show the same risk metrics now spatially aggregated over all schools (i.e. summing over the risk maps). This is done for each of the 12 UKCP18 ensemble members individually, and the distributions shown in the histograms quantify the ensemble spread across these 12 ensemble members.

As a validation of the UKCP18 estimated risk, an equivalent 'true' spatially aggregated risk is calculated based on observed hazard data (HadUK-Grid, Hollis et al., 2019), keeping the exposure and vulnerability consistent, as presented in Fig. 5 (c) and (g). This shows how the UKCP18 ensemble spread (the histogram) overlaps with this estimate of 'true' historical risk, with the ensemble mean lying very close to this value. A further validation is presented in Fig. 5 (d) and (h). This shows how the difference between UKCP18 ensemble mean risk and the 'true' historical risk at each school is consistently low across the study region (within 1–2 days for both overheating metrics).

The UKCP18 ensemble mean risk at each school is presented for each warming level and overheating threshold in Fig. 6. This shows how the risk of overheating in schools increases with increasing climate change warming level. When overheating is characterised by indoor temperature exceeding 26 °C, the number of days of overheating is generally consistent across the region (although slightly lower in the north and south-west), increasing from around 60 days per school year in the current climate to 90 days per school year in the 4 °C global warming level (i.e. a 50 % increase). Conversely, when overheating is characterised by indoor temperature exceeding 35 °C, the spatial variability in the risk is greater, and the relative change in the risk is greater, increasing in magnitude from approximately 4 days per year in the current climate to 24 days per year in the 4 °C global warming level in the most at-risk regions (i.e. a 600 % increase). While these results are based on a number of assumptions and caveats (see Section 4), they give an indication of the change of risk, and highlight the potentially significant influence climate change could have on the risk of overheating in schools, particularly at the high overheating threshold, which will have an important impact on the potential for learning during these hot days.

Fig. 7 (a) and (b) show the climate model ensemble mean and distribution of overheating risk (expected annual number of days of overheating) when aggregated over all schools, equivalent to Fig. 5 (c) and (g) but now for all three global warming levels. Consistent with the risk maps in Fig. 6, these show how overheating risk increases with global warming level for both overheating thresholds. Notably, the climate model ensemble spread remains relatively consistent across warming levels for the risk associated with exceedance of the 26 °C overheating threshold (the histogram range on the x axis is similar for the different warming levels), but this spread increases with warming level for the higher 35 °C overheating threshold (the histogram range on the x axis is much larger for the 4 °C warming level). This suggests that the climate projections are less certain (i.e., in less agreement) about how more extreme temperatures will change in the future compared to more moderate temperatures. This is a common feature of climate data, as rare extreme events are less well sampled and hence inherently more uncertain.

In addition, for comparison, Fig. 7 (a) and (b) show the equivalent climate model ensemble mean risk calculated using a non-spatially consistent 'regional location' representation of the hazard data. The risk assessment process described in Section 2 is applied to assess overheating risk in schools, but using hazard information from one location to represent the hazard felt by all locations within a given region. Specifically, the 13 regions shown in Fig. 2 (c) are used, and the regional location is specified as the central point by longitude and latitude (shown in Fig. 7 (f) of the Supplementary Material). This shows how, for all warming levels and both overheating thresholds, the 'regional location' approach underestimates the spatially aggregated overheating risk. This is particularly apparent for the 26 °C overheating threshold, where the 'regional location' estimate lies outside of the UKCP18 ensemble spread for all warming levels. This highlights how simplifying the hazard component of the risk and not capturing it in a spatially consistent way leads to a misrepresentation of risk (as has been shown by Sayers et al. (2023) for flood risk). For reference, plots equivalent to Fig. 6 for this non-spatially consistent 'regional location' approach are provided in Fig. 7 of the Supplementary Material.

Fig. 8 shows a more detailed spatial exploration of the difference between the risk estimated using the two hazard representations (for the 2 °C global warming level). These show more explicitly how using a hazard representation that is not fully spatially varying (i.e. the 'regional location' approach) leads to under and over estimation of risk across locations. For the 26 °C overheating threshold, the 'regional location' approach generally underestimates risk across schools, with a difference of up to 45 overheating days in the year in the north of England, explaining the overall large underestimation of the spatially aggregated risk in Fig. 7 (a). For the 35 °C

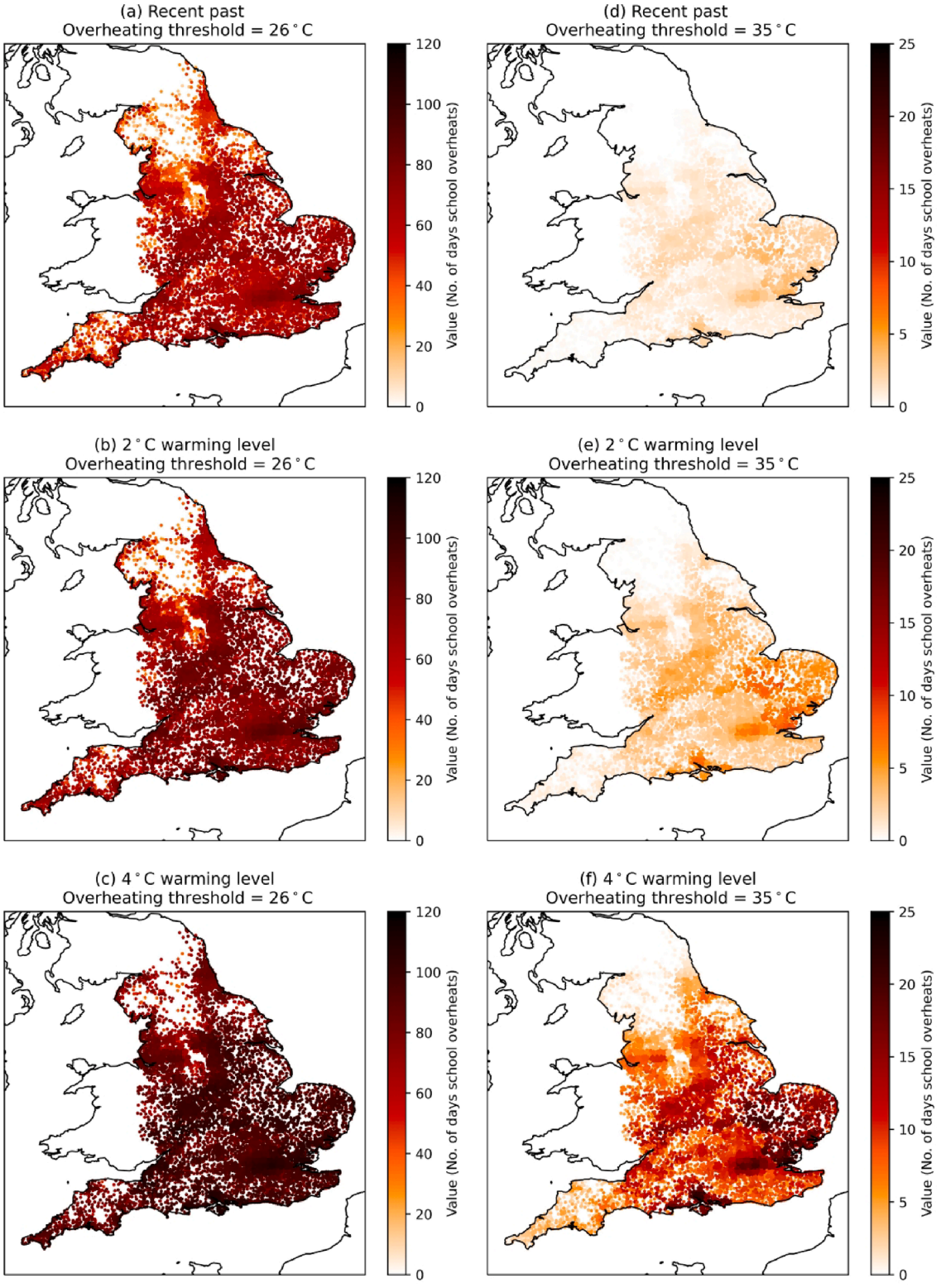

(caption on next page)

Fig. 6. A representation of future climate risk when applying the CLIMADA platform to the 12 UKCP18 ensemble members: For the 26 °C overheating threshold (a) the ensemble mean risk (expected annual total number of days each school overheats) associated with bias corrected UKCP18 for the current climate / recent past (i.e. the same as Fig. 5 b); (b) the ensemble mean risk associated with bias corrected UKCP18 for the 2 °C above pre-industrial global warming level; (c) the ensemble mean risk associated with bias corrected UKCP18 for the 4 °C above pre-industrial global warming level. Figures (d) (f) are as in (a) - (d) but for the 35 °C overheating threshold.

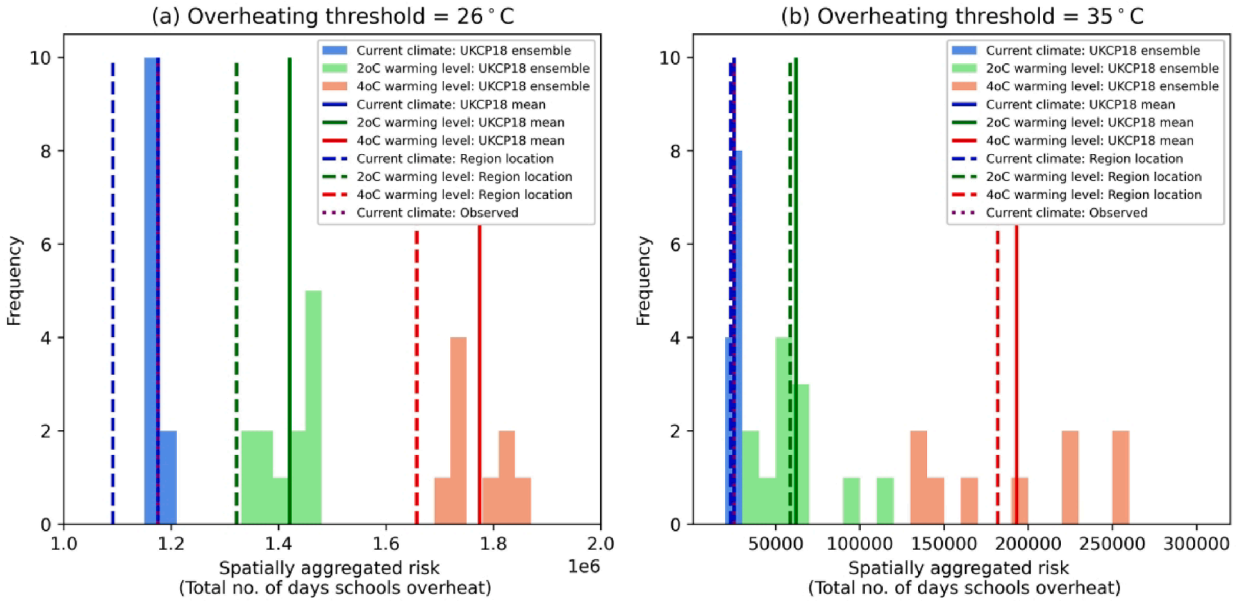

Fig. 7. A representation of spatially aggregated future climate risk when applying the CLIMADA platform to the 12 UKCP18 ensemble members: For the 26 °C overheating threshold (a) histograms showing the distribution of spatially aggregated risk across the 12 UKCP18 ensemble members for each warming level, with vertical lines included to show the UKCP18 ensemble mean, the equivalent risk metric calculated using the 'regional location' approach (see Section 3 of the Supplementary Material) and the equivalent for the 'observed' (HadUK-Grid) risk in the recent past; (b) the equivalent for the 35 °C overheating threshold.

overheating threshold, the overheating risk is generally underestimated in urban areas (particularly London, Southampton and Portsmouth, with a difference of up to 5.5 days) and overestimated in other regions. This is likely due to the geographical location of the 'regional location' used for demonstration in this study not being representative of higher temperatures associated with some urban geographies. This highlights how the seemingly relatively small difference between the UKCP18 and 'regional location' approaches in 7 (b) is in fact due to the counterbalance of positive and negative differences across different schools. Hence, this demonstrates that at both overheating thresholds there are important biases in the spatial and overall quantification of risk if the hazard is not represented as fully spatially varying. In particular, the overheating risk is likely to be underestimated in places where the hazard is most extreme and hence is potentially most important to capture accurately to inform adaptation prioritisation and decision making.

3.2. Results: generalised additive model (for risk)

The GAM structure described in Section 2.8 is used to model the UKCP18 ensemble of 12 risk maps, representative of each of the 3 warming levels and each of the 2 overheating thresholds (i.e. 6 separate GAMs are fitted). Validation plots, similar to those presented in Dawkins et al. (2023a), are shown in Section 2 of the Supplementary Material for each of these GAMs. These show good alignment between the modelled and simulated risk, indicating that the fitted GAMs are able to represent the climate projections well and can therefore be used to simulate additional risk maps to provide a richer quantification of climate model uncertainty (as described in Section 2.8).

For each of the GAMs, 1000 simulations of risk are generated for each school, providing a representation of the predictive distribution for risk at each school. This means that not only the ensemble mean and individual ensemble members can be presented, but rather a quantification of upper and lower prediction intervals for risk can be quantified, not possible if using the original 12 ensemble members only. As described by Dawkins et al. (2023a), this quantification of uncertainty is important for decision making, which should be based on as complete a range of plausible outcomes as possible, including the unlikely extremes. A demonstration of this improved uncertainty quantification is given in Figs. 9 and 10. These figures are equivalent to results in Figs. 6 and 7, but now the statistical modelling provides a much richer distribution for risk.

For the 26 °C overheating threshold, Fig. 9 (a) - (f) show relatively small climate model uncertainty in the overheating risk (compared to the mean risk) in the future global warming levels (+/- 5–15 days per year). Based on this model (keeping in mind the

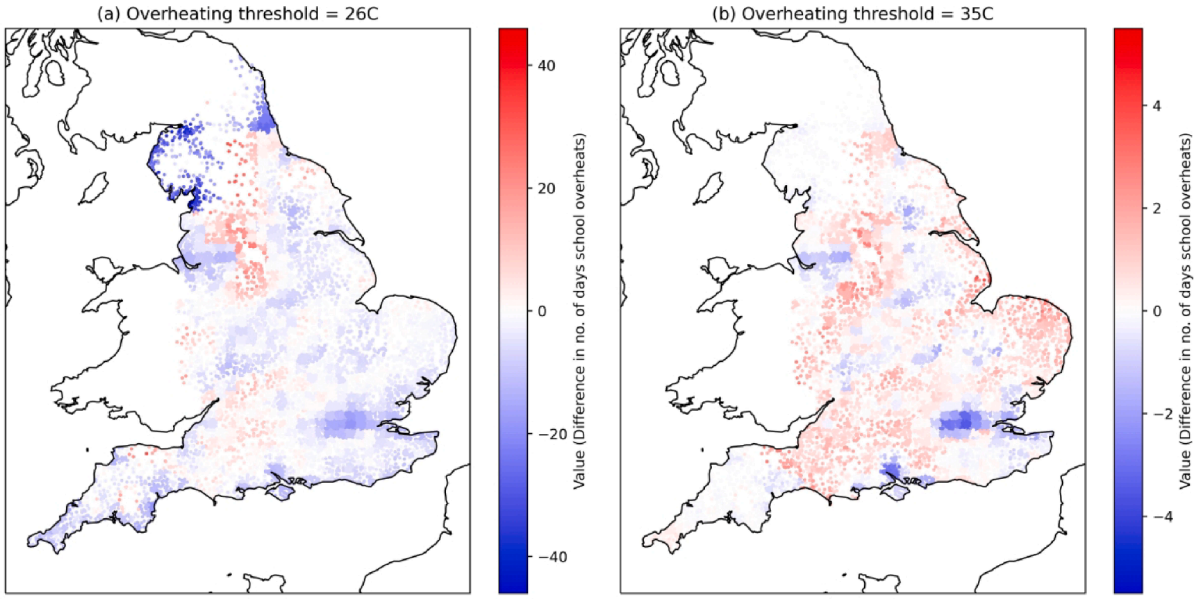

Fig. 8. An exploration of the difference between overheating risk (for the 2 °C global warming level) estimated using the two hazard representations (the 'regional location' approach and spatially varying gridded UKCP18 data), for (a) the 26 °C overheating threshold, and (b) the 35 °C overheating threshold. Negative values indicate that the 'regional location' approach underestimates risk when compared with the equivalent risk estimated using UKCP gridded data, and vice versa for positive values.

caveats and limitations), these results suggest with 95 % probability, that the most at-risk schools could overheat between approximately 80–100 days per school year (of 195 days) at the 2 °C global warming level, and 100–120 days per school year at the 4 °C global warming level. This analysis therefore suggests that, in the most at-risk schools, indoor thermal conditions could plausibly exceed the 26 °C overheating threshold on up to approximately 50 % and 60 % of school days at the 2 °C and 4 °C global warming levels respectively.

For the 35 °C overheating threshold, Fig. 10 (a) - (f) show relatively larger climate model uncertainty in the overheating risk (compared to the mean risk). These results suggest (again keeping in mind the caveats and limitations of the model),

with 95 % probability, that the most at-risk schools could overheat between approximately 5–15 days per school year at the 2 °C global warming level and 15–40 days per school year at the 4 °C global warming level. This analysis therefore suggests that, in the most at-risk schools, indoor thermal conditions could exceed the 35 °C overheating threshold on up to approximately 8 % and 20 % of school days at the 2 °C and 4 °C global warming levels respectively.

Fig. 9 (g) and Fig. 10 (g) show the equivalent distributions for spatially aggregated risk to those shown in Fig. 7, now with the distribution from the 1000 GAM simulated ensemble members added. These show how the GAM is able to sample plausible outcomes that align well with the original 12-member climate projection ensemble, while also adding a richer quantification of the risk distributions, particularly the upper and lower tails. As mentioned previously, there is larger climate model uncertainty in the exceedance of the higher overheating threshold. This is due to the occurrence of rare extremes being relatively less sampled by the climate data. The uncertainty/spread in the individual ensemble members (as seen in Fig. 7 b) is reflected in the subsequent GAM samples (Fig. 10 g), as this is captured by the ensemble member random effect (see Section 2.8). Summary statistics for the England area aggregate values show in 9 and 10 are given in Table 2.

Fig. 9 (g) suggests that, at the 4 °C global warming level, across the ~20,000 schools included, there could plausibly be 1.9 million days of overheating in a school year at the 26 °C overheating threshold (approximately 50 % of potential days across all schools). Equivalently, Fig. 10 (g) suggests that, at the 4 °C global warming level, across the ~20,000 schools included, there could plausibly be 300,000 days of overheating in a school year at the 35 °C overheating threshold (approximately 8 % of potential days across all schools).

Again, it is important to note that these figures are derived based on a number of modelling assumptions and known caveats, and are based on the south facing classroom orientation which is likely to experience the hottest temperatures. As such, further work to refine the approach and test sensitivities (e.g. as in Dawkins et al., 2023b) should be undertaken, and the figures presented here should not be quoted out of context. This analysis does, however, provide an initial indication of how overheating risk may change in plausible future climates.

3.3. Results: Prioritising adaptation

Often, the aim of a spatial climate risk assessment is to identify which of the spatially distributed assets/exposures are most at risk

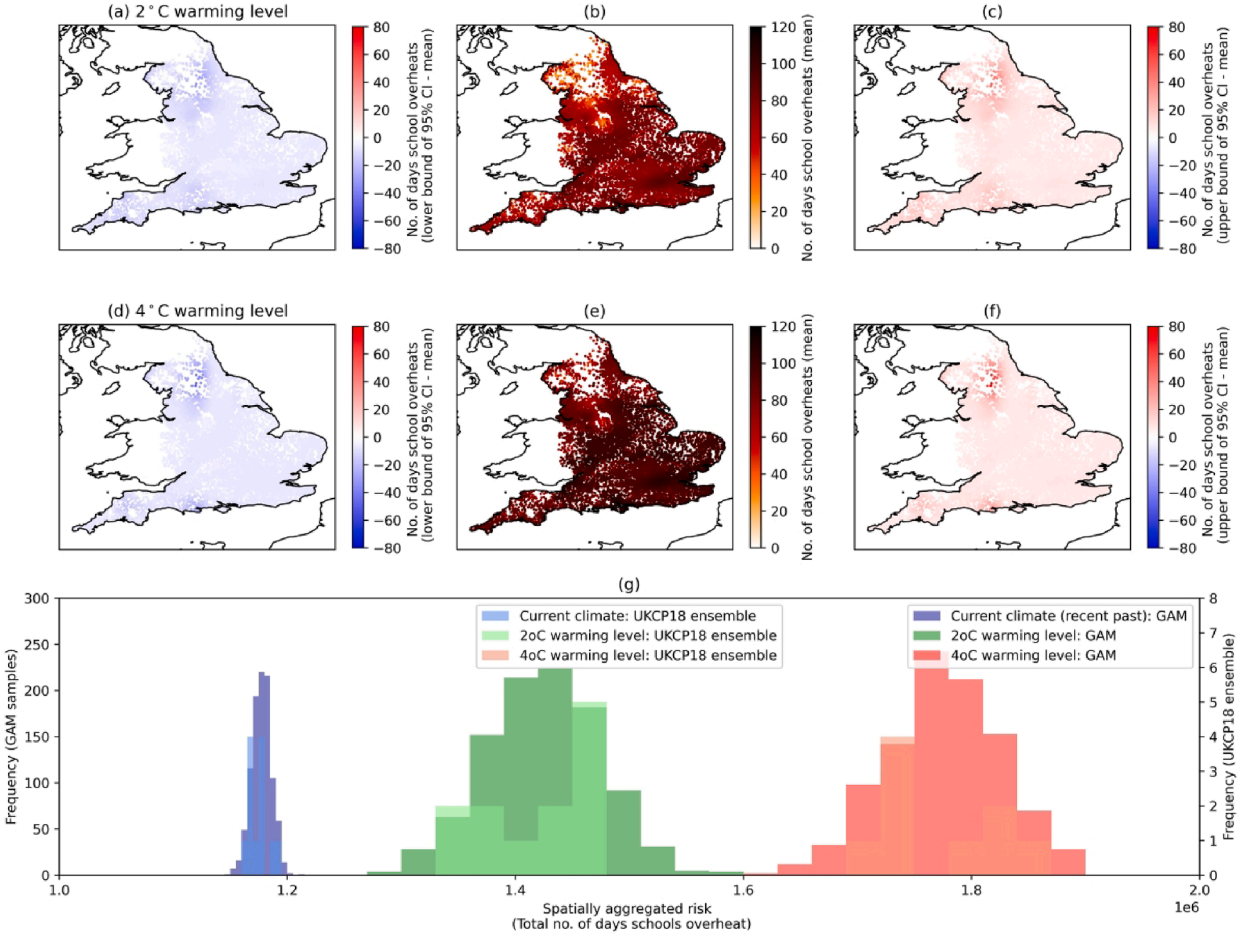

Fig. 9. The quantification of overheating risk in schools enabled by the statistical modelling framework, using the 1000 samples generated from the GAM for each warming level and the 26 °C overheating threshold: For the 2 °C above pre-industrial global warming level (a) the lower bound of the 95% prediction interval of risk (expected annual total number of days each school overheats) minus mean risk; (b) mean risk; and (c) the upper bound of the 95% prediction interval of risk minus mean risk; Plots (d) - (f) are the same as (a) - (c) but for the 4 °C above pre-industrial global warming level; (g) histograms showing the distribution of spatially aggregated risk across the 1000 GAM samples for each warming level. The equivalent histograms for the 12 UKCP18 ensemble members (as in Fig. 7) are included as a comparison.

and should therefore be prioritised when planning climate adaptation.

Fig. 11 shows a demonstration of how the results of a spatial climate risk assessment, such as this, could be used to this end. Fig. 11 (a) shows how each school can be assigned to a risk category (Low/Medium/High). The example here shows a certain specification of these categories (detailed in the bullet points below), but in a real-world situation these figures would be selected according to the specific policy context.

Here, this risk categorisations is based on the GAM simulated ensemble mean risk (expected annual total number of days the school overheats) for the 35 °C overheating threshold and the 2 °C global warming level, such that:

- Low risk: the lowest 80 % of schools in the risk metric (i.e. below the 80th percentile of the risk metric),
- Medium risk: schools between the 80th-90th percentile of the risk metric,
- High risk: the top 10 % of schools in the risk metric (i.e. above the 90th percentile of the risk metric).

Note that this categorisation approach has been fabricated for demonstrative purposes, and does not reflect an approach that would be used in a real-world application. Alternative risk metrics, summary statistics of the predictive distribution of risk, overheating thresholds, global warming levels and categorisations could be used, and exploring alternatives will give a greater understanding of the stratification of the risk categories across the exposed assets (providing a more robust insight). Fig. 11 (b) shows a subset of the points in (a), here just for the Thames Valley region. Exploration of this plot in combination with Fig. 11 (c) and Fig. 4 (c) provides insights into how the hazard, exposure and vulnerability components relate to the risk categories.

Specifically, 11 (c) shows how the proportion of schools in the medium and high risk categories generally increases for newer

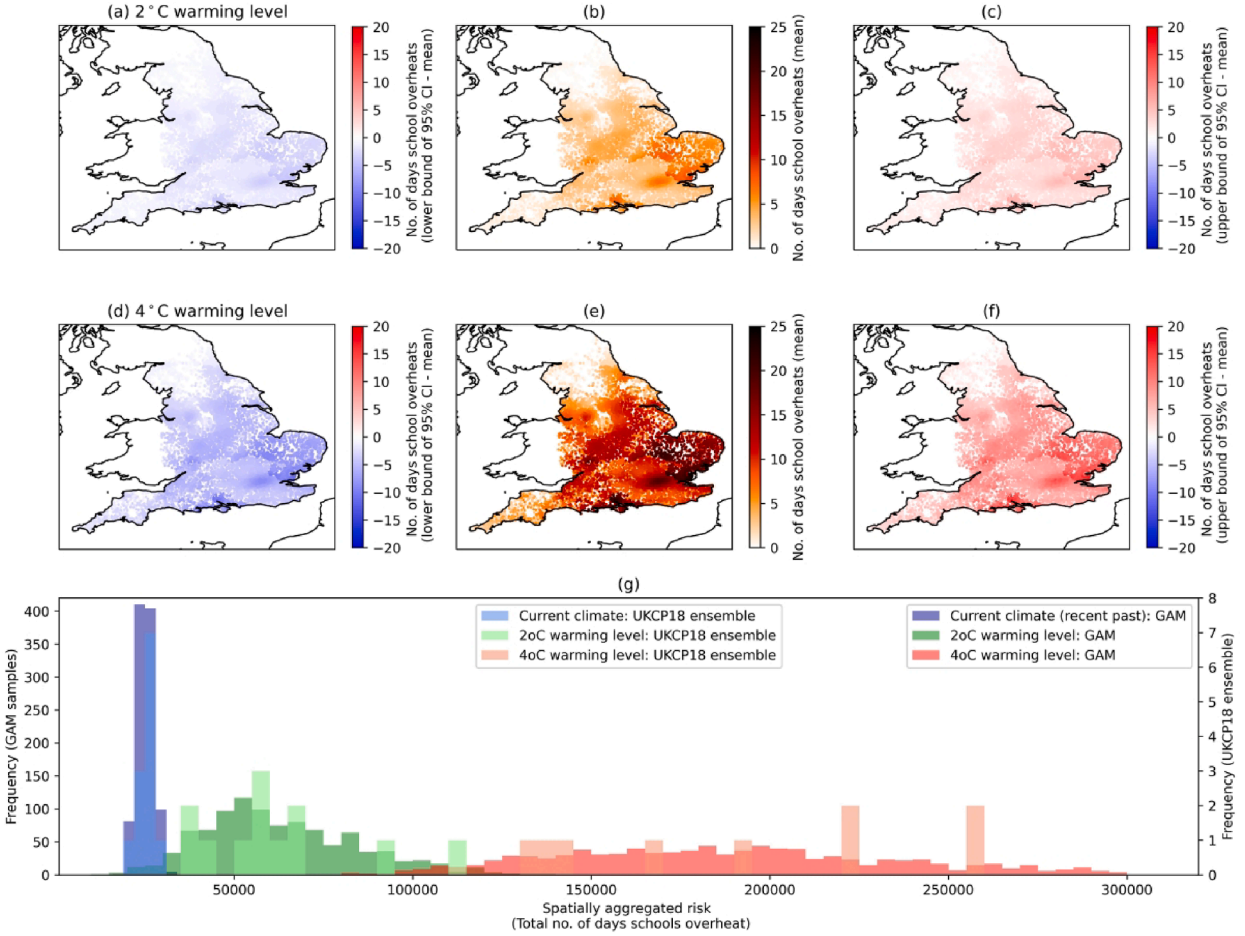

Fig. 10. As in Fig. 9 but for the 35 °C overheating threshold risk metric.

Table 2
Summary statistics representing the distribution of risk (annual expected number of schools overheating) calculated using 1000 samples generated from the GAM. The 10th, median (50th) and 90th percentiles of England-wide, spatially aggregated risk are presented for each of the warming levels for both the 26 °C and 35 °C overheating thresholds.

	Current	Current	Current	2 °C	2 °C	2 °C	4 °C	4 °C	4 °C
	10th	Median	90th	10th	Median	90th	10th	Median	90th
26 °C	1,166,389	1,177,949	1,188,353	1,361,370	1,424,985	1,489,070	1,706,591	1,776,796	1,842,398
35 °C	22,297	25,053	28,061	38,191	59,415	92,895	127,292	187,024	268,569

building era categories (i.e. relatively more high risk schools are newer schools), with similar proportions for the two education stages (primary and secondary). Indeed, in the Thames Valley region, all pre-1918 schools are in the low risk category. Further, comparing Fig. 11 (b) and Fig. 4 (c) shows that, while there are post-1976 schools distributed across the region, only those in the greater London region are categorised as medium and high risk. This highlights how the higher hazard intensity in this urban area (e.g. as seen in Fig. 4 a) also contributes to the spatial variability in the risk categorisation (likely due to the urban heat island effect). This is further demonstrated by identifying the equivalent categorisations using risk derived from the 'regional location' hazard representation, for which all of the Thames Valley region schools are categorised as 'Low risk' (see Fig. 8 in the Supplementary Material). This highlights how the risk categorisations are very sensitive to the representation of the hazard, and again the potential to underestimate risk in high-risk regions if this 'regional location' approach is used.

Finally, Fig. 11 (d) shows how risk categorisations could be displayed on a street map for ease of interpretation and visualisation. Future work could aim to provide such information on a map in an interactive data portal, such as the ArcGIS based Met Office Climate Data Portal (https://climate-themetoffice.hub.arcgis.com/), allowing schools to interact with the outputs and explore their individual place-based climate risk. This could help inform school specific climate adaptation planning.

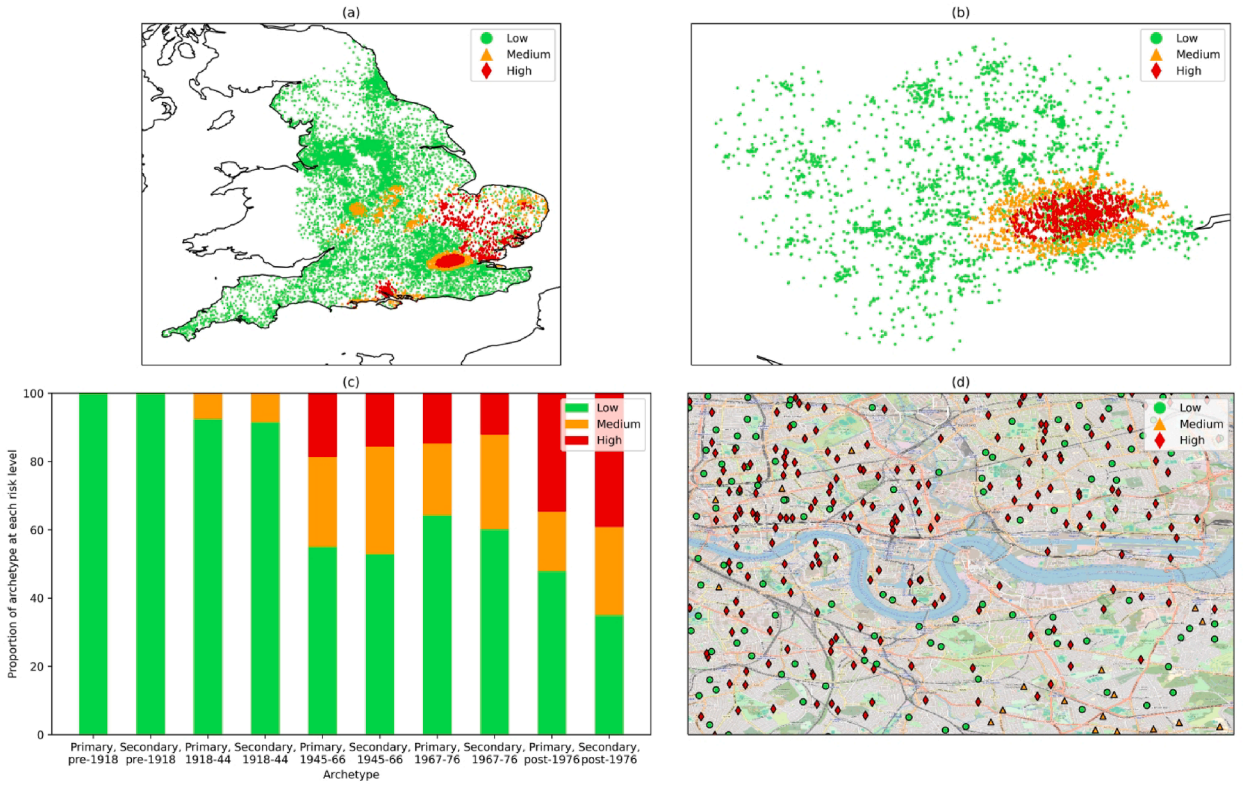

Fig. 11. A demonstration of how the outputs from the spatial climate risk assessment framework applied in this study can be used to prioritise, explore and visualise the most at-risk schools: (a) a map of risk categorisations based on the fabricated approach described in the text; (b) a subset of the map of risk categorisations, for the Thames Valley region only; (c) a bar chart showing the proportion of low, medium and high risk schools in each of the school building archetypes in the Thames Valley region; and (d) a street map visualisation of risk categorisations in central London.

4. Limitations

There are a number of ways in which the analysis presented in this study could be improved upon in future iterations or in alternative applications (i.e., to other sectors).

Firstly, the study only considers one set of input factors related to the hazard, exposure and vulnerability (apart from the three warming levels). Specifically, only the UKCP18 regional climate hazard data source is considered, one representation of the school archetypes, and one set of vulnerability functions. As discussed in Dawkins et al. (2023b), undertaking a risk assessment requires the modeller to make many (largely subjective) choices, such as which hazard, exposure and vulnerability data to use. Hence, alternative options should be considered to understand the uncertainty and sensitivity of risk to these input choices. Future work should aim to undertake an uncertainty and sensitivity analysis for this application to further quantify the uncertainty in the risk and help inform transparent and robust adaptation decision making.

In addition, the climate data used within this study is provided on a 12 km spatial grid. This means that, while this spatial representation of the hazard is an improvement upon the 'regional location' approach, the 12 km grid cells are unlikely to capture the local conditions felt at a particular school. To improve upon this, higher resolution climate projections could be employed, such as the world leading high resolution 2.2 km convection-permitting model projections, recently updated as part of UKCP18.

The approach taken for representing the vulnerability of schools to overheating could be improved upon. In this application schools are categorised as one of a number of building archetypes, and the same vulnerability function is used to represent all schools of the same archetype. In reality, each school will have a different thermal response to outdoor meteorological conditions and hence the vulnerability function should vary on a school-by-school basis. Indeed, this will also likely vary for the different buildings that make up each school, and the different orientations of different classrooms (here only the south facing orientation is considered in the results). Building-by-building school models have been developed (MPS, the Modelling Platform for Schools, Schwartz et al., 2022), and hence work is ongoing to explore the application of this data. Further, in this study, the detailed building simulation data is modelled using a simple linear function between outdoor and indoor temperature. While the validation of this linear relationship (e.g. Fig. 3) shows a good fit, there is variability in the indoor temperature for a given outdoor temperature that is not captured by a single linear fit, and hence this is lost in the analysis. Moreover, this function only captures the relationship between outdoor and indoor temperature and therefore does not capture the additional effect of other meteorological variables (e.g. solar radiation and humidity). Future work could look to include these additional variables within the analysis which may help to capture more of the variability in the outdoor-

indoor temperature relationship.

Here, the risk assessment considers only a simple overheating threshold within the impact and risk metrics. More work is required to understand how the exceedance of such thresholds (and event the length of such hot spells) causes tangible impact, such as the impact on health, well-being, learning potential and exam attainment. Further, the method for evaluating overheating could also be adjusted, to align with the guidance for schools in BB101 (Education & Skills Funding Agency, 2018), which uses a variable threshold through the year, rather than a constant one, to define overheating. In addition, there are a selection of studies that explore the relationship between indoor temperature and cognitive performance (e.g. Wargocki et al., 2019). These insights could be built into future iterations of this application. However, further studies, data and insights may need to be gathered to make these representations of impact/risk more robust and user specific. Further, in this application the risk is given for each school as a whole, whereas it is likely that the urgency in adapting, and hence the risk is also a function of the number of pupils at the school, as well as possibly information about the vulnerability of the pupils (e.g., pre-existing health conditions). Future work should also look to include these factors within the risk quantification.

Finally, the current study does not provide insights into the potential benefits of different passive or active adaptation approaches, such as the increased use of mechanical ventilation, or night-time venting. Building models are a valuable tool for testing such approaches, as was done by Grassie et al. (2023). A valuable direction of future work could therefore re-apply the spatial risk assessment approach presented in this study, but using adapted building simulations for the same schools. The results could then be compared with those presented here to explore which adaptation measures are best at reducing the risk (i.e. number of days of overheating).

5. Implications for risk management

This study provides some useful insights for those concerned with climate risk management and adaptation decision making. Specifically, the value of using open-source risk assessment frameworks as a tool for *spatially coherent* risk quantification. As discussed in the Introduction, this spatial coherence is important for organisations with spatially distributed assets who wish to understand the relative magnitude of the risk at these different sites (e.g. to prioritise adaptation action to those most at risk). This is also shown to be important when aggregating risk over space. Throughout, this is evidenced by comparing risk estimated using spatially varying hazard information taken from gridded climate projections and estimated using just one 'regional location' from the climate projections to represent the hazard at all locations in that region (as is often done in overheating climate impact analyses e.g. Arup, 2022; DLUHC, 2019; Tsoulou et al., 2022; Dong et al., 2023b).

As discussed in Dawkins et al. (2023a), the additional uncertainty quantification enabled by the statistical modelling step provides many more plausible realisations of risk at each location. This helps to inform climate risk management about locations where risk could plausibly be much higher or lower than when quantified using just the limited climate model ensemble, which may be relevant for planning and decision making. It is important to note, however, that this must not be interpreted as a full quantification of uncertainty, but is just a richer representation of the climate model ensemble uncertainty. This is conditional on all of the other subjective choices that have been made in the risk calculation, and a fuller picture of the uncertainty would be understood through varying the input of the risk assessment in a meaningful way (as in Dawkins et al. (2023b)).

The quantification of the vulnerability function is often very challenging. This application provides an example of using insights from disciplines outside of climate science to infer the vulnerability, drawing from building science (Grassie et al., 2023) to infer the building overheating vulnerability (using models developed based on large data collection and survey initiative by the Department for Education). As discussed in the previous section, however, quantifying tangible impacts in specific climate risk management applications (e.g. loss of learning, health, well-being) requires the user to have the data and/or insights required for estimating such impacts. This information is often limited, and advances in climate risk assessment and management depend on organisations gathering such data and insights. Hence, while obtaining this information is a large undertaking, it is vital for an informative assessment of real-world impacts.

6. Conclusion

This study has presented a novel application of the CLIMADA risk assessment platform and extended framework of Dawkins et al. (2023a), to assess overheating risk in schools. This application demonstrates the advantages of bringing together open-source spatial risk assessment frameworks, data science techniques, and physics-based building models to assess climate risk associated with overheating in buildings in a spatially consistent way. This allows for the identification of the most at risk assets/exposures, based on a richer quantification of climate model uncertainty.

We show how hazard (temperature) information from an ensembles of climate projections can be combined with information about the exposure (location) and vulnerability (thermal response) of ~20,000 schools in England, to provide a spatially coherent representation of risk (the expected number of days each school will overheat in a year) in different plausible climates. This is achieved by using the relationship between outdoor and indoor thermal conditions from physics-based building model simulations to inform the characterisation of the vulnerability component of the risk assessment.

We show how the (bias corrected) UKCP18 RCM ensemble validates well against observation datasets in terms of overheating risk in schools in the recent past, both in individual locations and accumulated over schools. Conversely, we show how using the 'regional location' hazard representation approach (where one location is used to represent the hazard for all schools in a given region, as in a number of recent overheating studies), leads the risk being over- and under-estimated across locations. This highlights how simplifying the hazard component of the risk and not capturing it in a spatially consistent way leads to a misrepresentation of risk, meaning the

results cannot be used to compare and prioritise assets/exposures or estimate national accumulated risk (similar to the conclusions of Sayers et al. (2023) for flood risk).

In future climates, representing global warming levels of 2 °C and 4 °C above pre-industrial, this novel application indicates an increase in the risk of overheating in schools. Specifically, when overheating is characterised as indoor operative temperature exceeding 26 °C, there is approximately a 50 % increase in the annual expected number of days of overheating in the most at risk schools (between the current day climate a the 4 °C warming level). Further, when overheating is characterised as indoor operative temperature exceeding 35 °C, there is approximately a 600 % increase in the most at risk schools. This indicates that the relative frequency of very hot days may increase more than moderately hot days, which may have important impacts on the potential for learning. Due to the limitations and caveats associated with this study (see Section 4), these figure should not be considered as a final estimate, but more an indication of the change in risk in the future, and something to build upon in future risk assessments.

Similar to Dawkins et al. (2023a), we show how a GAM, involving an 'ensemble member' random effect term, can be used to statistically represent the ensemble summary of risk and be used to simulate many more realisations of risk, representative of a larger collection of plausible ensemble members (e.g. 1000 rather than 12). We demonstrate how this approach provides a richer quantification of the uncertainty in risk, particularly in the upper and lower tails of the risk distribution. It should be noted, however, that when the climate model ensemble is known to structurally miss some of the uncertainty (as is often the case), simulations from the GAM will also suffer this problem and to overcome this, the GAM should be used to model ensemble members from many different structurally different climate models as hazard data sources.

Finally, we present a demonstration of how the results of a spatial risk assessment such as this can be used to prioritise exposed assets based on their assessed risk. In this application, this allows for individual school-level categorisation of risk level (low, medium and high), which can be related back to the characteristics of the school and the influence of the spatially varying hazard conditions. In future, such information could be incorporated into an interactive data portal to allow schools to interact with the outputs and explore their individual place-based climate risk. This could help inform school-specific climate adaptation planning.

There are a number of limitations to the application presented, as described in Section 4. Future work should focus on addressing these. In particular, the spatial granularity of the risk assessment could be enhanced by implementing the recently updated UKCP18 high-resolution 2.2 km convection-permitting model projections within the hazard component, and buildingby-building school building models (e.g. of Schwartz et al. (2022)) within the vulnerability component. Comparing the risk assessment here with the results from this alternative input setting (as well as other potential combinations of hazard, exposure and vulnerability) will also provide valuable insight into the uncertainty and sensitivity of the results to these subjective modelling choices, which will be important for informing robust adaptation decision making, as discussed by Dawkins et al. (2023b). Further, this approach has the potential to be applied to other regions, hazards or risk metrics of interest (provided suitable data is available), which in the case of UK government, could provide insight to inform transparent and robust adaptation decision making as part of NAP3, and spatial risk assessments in CCRA4.

CRediT authorship contribution statement

Laura C. Dawkins: Writing – original draft, Visualization, Validation, Software, Methodology, Formal analysis, Conceptualization. **Kate Brown:** Writing – original draft, Visualization, Validation, Software, Methodology, Formal analysis. **Dan J. Bernie:** Conceptualization, Supervision, Writing – review & editing. **Jason A. Lowe:** Writing – original draft. **Theodoros Economou:** Methodology. **Duncan Grassie:** Writing – original draft, Formal analysis, Data curation. **Yair Schwartz:** Writing – original draft, Methodology, Formal analysis, Data curation. **Daniel Godoy-Shimizu:** Writing – review & editing, Writing – original draft, Methodology, Formal analysis, Data curation. **Ivan Korolija:** Data curation. **Dejan Mumovic:** Investigation. **David Wingate:** Writing – review & editing. **Emma Dyer:** Visualization.

Declaration of competing interest

The authors declare that they have no known competing financial interests or personal relationships that could have appeared to influence the work reported in this paper.

Data availability

Data will be made available on request.

Acknowledgements

This work (and the time of L.D., K.B, D.B. and J.L.) was funded under the Strategic Priority Fund for UK Climate Resilience. The UK Climate Resilience programme is supported by the UKRI Strategic Priorities Fund. The programme is co-delivered by the Met Office and NERC on behalf of UKRI partners AHRC, EPSRC and ESRC. T.E. was funded by the European Union's Horizon 2020 research and innovation programme under grant agreement No. 856612 https://ec.europa.eu/info/research-and-innovation/funding/funding-opportunities/funding-programmes-and-open-calls/horizon-europe_en and the Cyprus Government. The building modelling study was funded by an Engineering and Physical Sciences Research Council (EPSRC) grant, 'Advancing School Performance: Indoor Environmental Quality, Resilience and Educational Outcomes' (ASPIRE, EP/T000090/1). The authors gratefully acknowledge the

supply of data and support by the Department for Education.

Appendix A. Supplementary data

Supplementary data to this article can be found online at https://doi.org/10.1016/j.crm.2024.100602.

References

Angelov, P., Soares, E., Jiang, R., Arnold, N., Atkinson, P., 2021. Explainable Artificial Intelligence: An Analytical Review. Data Mining and Knowledge Discovery, Wiley Interdisciplinary Reviews, p. 11.

Arnell, N., Kay, A., Freeman, A., Rudd, A., Lowe, J., 2021. Changing climate risk in the UK: a multi-sectoral analysis using policy-relevant indicators. Clim. Risk Manag. 31, 100265.

Arup, 2022. Addressing overheating risk in existing UK homes. Tech. Rep.

Aznar-Siguan, G., Bresch, D.N., 2019. CLIMADA v1: a global weather and climate risk assessment platform. Geosci. Model Devel. 12, 3085–3097.

Betts, R.A., Brown, K., 2021. Introduction. The Third UK ClimateChange Risk Assessment. Technical report.

Betts, R., Haward, A., Pearson, K., 2021. The third UK climate change risk assessment technical report. Prepared for the Climate Change Committee, London.

Cibse, 2008. TM46: energy benchmarks. Tech. Rep.

Clark, K.M., 2002. The use of computer modeling in estimating and managing future catastrophe losses. The Geneva Papers on Risk and Insurance 27 (2), 181–195.

Crespi, A., Renner, K., Zebisch, M., Schauser, I., Leps, N., Walter, A., 2023. Analysing spatial patterns of climate change: climate clusters, hotspots and analogues to support climate risk assessment and communication in Germany. Clim. Serv. 30, 100373.

Dawkins, L.C., Bernie, D.J., Lowe, J.A., Economou, T., 2023a. Assessing climate risk using ensembles: a novel framework for applying and extending open-source climate risk assessment platforms. Clim. Risk Manag. 40, 100510.

Dawkins, L.C., Bernie, D.J., Pianosi, F., Lowe, J.A., Economou, T., 2023b. Quantifying uncertainty and sensitivity in climate risk assessments: varying hazard, exposure and vulnerability modelling choices. Clim. Risk Manag. 40, 100511.

Defra, 2023. The third National Adaptation Programme (NAP3) and the fourth strategy for climate adaptation reporting. Tech. Rep.

Department for Education (2017). Get information about schools. https://www.gov.uk/guidance/get-information-about-schools. Accessed: 2023-09-28.

DFE, 2023. Sustainability and climate change: a strategy for the education and children's services systems. https://www.gov.uk/government/publications/sustainability-and-climate-change-strategy/sustainability-and-climate-change-a-strategy-for-the-education-and-childrens-services-syst. Accessed: 2024-03-02.

DLUHC, 2019. Department for levelling up housing and communities (formally ministry og housing communities and local government): research into overheating in new homes. Tech. Rep.

Dong, J., Schwartz, Y., Korolija, I., Mumovic, D., 2023a. The impact of climate change on cognitive performance of children in english school stock: a simulation study. Build. Environ. 243, 110607.

Dong, J., Schwartz, Y., Mavrogianni, A., Korolija, I., Mumovic, D., 2023b. A review of approaches and applications in building stock energy and indoor environment modelling. Build. Serv. Eng. Res. Technol. 44 (3), 333–354.

Economou, T., Lazoglou, G., Tzyrkalli, A., Constantinidou, K., Lelieveld, J., 2023. A data integration framework for spatial interpolation of temperature observations using climate model data. PeerJ 11, e14519.

Education & Skills Funding Agency, 2016. Priority school building programme: overview. https://www.gov.uk/government/publications/psbp-overview/priority-school-building-programme-overview. Accessed: 2023-09-28.

Education & Skills Funding Agency, 2018. Building bulletin 101: Guidelines on ventilation, thermal comfort and indoor air quality in schools: Version 1. Technical report.

Environment Agency, 2009. Flooding in England: A National Assessment of Flood Risk. Technical report.

Garry, F.K., Bernie, D.J., Davie, J.C.S., Pope, E.C.D., 2021. Future climate risk to UK agriculture from compound events. Clim. Risk Manag. 32, 100282.

Gelman, A., Carlin, J.B., Stern, H.S., Dunson, D., Vehtari, A., Rubin, D.B., 2014. Bayesian Data Analysis, third ed. Chapman & Hall/CRC, Boca Raton, Florida, USA.

Godoy-Shimizu, D., Hong, S., Korolija, I., Schwartz, Y., Mavrogianni, A., Mumovic, D., 2022. Pathways to improving the school stock of England towards net zero. Build. Cities 3 (1), 939–963.

Grassie, D., Schwartz, Y., Symonds, P., Korolija, I., Mavrogianni, A., Mumovic, D., 2022. Energy retrofit and passive cooling: overheating and air quality in primary schools. Build. Cities 3 (1), 204–225.

Grassie, D., Dong, J., Schwartz, Y., Karakas, F., Milner, J., Bagkeris, E., Chalabi, Z., Mavrogianni, A., Mumovic, D., 2023. Dynamic modelling of indoor environmental conditions for future energy retrofit scenarios across the UK school building stock. J. Build. Eng. 63 (A), 105536.

Hanlon, H.M., Bernie, D., Carigi, G., Lowe, J.A., 2021. Future changes to high impact weather in the UK. Clim. Change 116, 50.

Hawchar, L., Naughton, O., Nolan, P., Stewart, M.G., Ryan, P.C., 2020. A GIS-based framework for high-level climate change risk assessment of critical infrastructure. Clim. Risk Manag. 29, 100235.

Hollis, D., McCarthy, M., Kendon, M., Legg, T., Simpson, I., 2019. HadUK-grid: a new UK dataset of gridded climate observations. Geosci. Data J. 6, 151–159.

IPCC (2022). Climate Change 2022: Impacts, Adaptation, and Vulnerability. Contribution of Working Group II to the Sixth Assessment Report of the Intergovernmental Panel on Climate Change [H.-O. Pörtner, D.C. Roberts, M. Tignor, E.S. Poloczanska, K. Mintenbeck, A. Alegría, M. Craig, S. Langsdorf, S. Löschke, V. Möller, A. Okem, B. Rama (eds.)]. Technical report.

Iturbide, M. et al., 2021. Repository supporting the implementation of fair principles in the ipcc-wg1 atlas. zenodo. https://github.com/IPCC-WG1/Atlas. Accessed: 2022-05-25.

Johnson, H., Kovats, S., McGregor, G., Stedman, J., Gibbs, M., Walton, H., 2005. The impact of the 2003 heat wave on daily mortality in England and Wales and the use of rapid weekly mortality estimates. Eurosurveillance 10 (7), 558.

Kovats, S., Brisley, R., 2021. Health, communities and the built environment. Tech. Rep.

Lan, C., Wild, A., Paulik, R., Wotherspoon, L., Zorn, C., 2023. Assessing indirect impacts of extreme sea level flooding on critical infrastructure. J. Marine Sci. Eng. 11 (7), 1420.

Lowe, J.A., et al., 2018. UKCP18 science overview report. Tech. Rep.

Mayor of London, 2020. How london schools and early years settings can adapt to climate change. https://www.london.gov.uk/sites/default/files/gla_schools_adaptation_guidance_14-10-20_issue.pdf. Accessed: 2024-03-02.

Met Office Hadley Centre, 2019. UKCP18 Convection-Permitting Model Projections for the UK at 2.2km resolution. NERC EDS Centre for Environmental Data Analysis. http://catalogue.ceda.ac.uk/uuid/ad2ac0ddd3f34210b0d6e19bfc335539. Accessed: 2023-09-29.

Murphy, J., Harris, G., Sexton, D., Kendon, E., Bett, P., Clark, R., Yamazaki, K., 2019. Ukcp18 land projections: science report. Tech. Rep.

Mylona, A., 2012. The use of UKCP09 to produce weather files for building simulation. Build. Serv. Eng. Res. Technol. 33 (1), 51–62.

Oikonomou, E., Mavrogianni, A., Jain, N., Gupta, R., Wilkinson, P., Howard, A., and Milojevic, A. (2020). Assessing heat vulnerability in london care settings: case studies of adaptation to climate change. https://discovery.ucl.ac.uk/ id/eprint/10128385/. Accessed: 2024-03-02.

Nikulin, G., et al., 2018. The effects of 1.5 and 2 degrees of global warming on Africa in the CORDEX ensemble. Environ. Res. Lett. 13 (6), 065003.

Paulik, R., Horspool, N., Woods, R., Griffiths, N., Beale, T., Magill, C., Wild, A., Popovich, B., Walbran, G., Garlick, R., 2022. RiskScape: a flexible multi-hazard risk modelling engine. Nat. Hazards 1573.
Petitti, D.B., Hondula, D.M., Yang, S., Harlan, S.L., Chowell, G., 2016. Multiple trigger points for quantifying heat-health impacts: new evidence from a hot climate. Environ. Health Perspect. 124 (2), 176–183.
Riahi, K., Rao, S., Krey, V., Cho, C., Chirkov, V., Fischer, G., Kindermann, G., Nakicenovic, N., and Rafaj, P. (2011). RCP 8.5—A scenario of comparatively high greenhouse gas emissions. Climatic Change, 109 (1-2):33–57.
Sayers, P., Griffin, A., Lowe, J., Bernie, D., Carr, S., Kay, A., Stewart, L., 2023. Beyond the local climate change uplift – the importance of changes in spatial structure on future fluvial flood risk in great britain. Nat. Hazards. https://doi.org/10.1007/s11069-023-06350-x.
Schleussner, C.F., Lissner, T.K., Fischer, E.M., et al., 2016. Differential climate impacts for policy-relevant limits to global warming: the case of 1.5C and 2C. Earth Syst. Dyn. 7 (2), 327–351.
Schwartz, Y., Korolija, I., Godoy-Shimizu, D., Hong, S.M., Dong, J., Grassie, D., Mavrogianni, A., Mumovic, D., 2022. Modelling platform for schools (mps): the development of an automated one-by-one framework for the generation of dynamic thermal simulation models of schools. Energ. Buildings 254, 111566.
Simpson, G., 2022. Using random effects in gams with mgcv. https://fromthebottomoftheheap.net/2021/02/02/random-effects-in-gams/. Accessed: 2022-05-23.
Stalhandske, Z., Nesa, V., Zumwald, M., Ragettli, M.S., Galimshina, A., Holthausen, N., Röösli, M., Bresch, D.N., 2022. Projected impact of heat on mortality and labour productivity under climate change in Switzerland. Nat. Hazards Earth Syst. Sci. 22, 2531–2541.
Steptoe, H., Economou, T., 2021. Extreme wind return periods from tropical cyclones in Bangladesh: insights from a high-resolution convection-permitting numerical model. Nat. Hazards Earth Syst. Sci. 21, 1313–1322.
Steptoe, H., Economou, T., 2023. Proliferation of atmospheric datasets can hinder policy making: a data blending technique offers a solution. Front. Big Data 6.
Strauss, B.H., Orton, P.M., Bittermann, K., Buchanan, M.K., Gilford, D.M., Kopp, R.E., Kulp, S., Massey, C., de Moel, H., Vinogradov, S., 2021. Economic damages from hurricane sandy attributable to sea level rise caused by anthropogenic climate change. Nat. Commun. 12 (2729).
Switanek, M.B., Troch, P.A., Castro, C.L., Leuprecht, A., Chang, H.I., Mukherjee, R., Demaria, E., 2017. Scaled distribution mapping: a bias correction method that preserves raw climate model projected changes. Hydrol. Earth Syst. Sci. 21, 2649–2666.
Taylor, T., 2021. Overheating risk under future climate scenarios: Climate change adaptation for schools. proceedings of 'lcaw schools summit: Climate resilient schools'. https://climatelondon.org/wp-content/uploads/2021/07/Tim-Taylor-LCAW-Schools-June-2021.pdf. Accessed: 2024-03-02.
Thompson, R., Landeg, O., Kar-Purkayastha, I., Hajat, S., Kovats, S., O'Connell, E., 2022. Heatwave mortality in summer 2020 in England: an observational study. Int. J. Environ. Res. Public Health 19 (6123).
Thompson, E.L., Smith, L.A., 2019. Escape from model-land. Economics 13 (405).
Tsoulou, I., Jain, N., Oikonomou, E., Petrou, G., Howard, A., Gupta, R., Mavrogianni, A., Milojevic, A., Wilkinson, P., Davies, M., 2022. Assessing the current and future risk of overheating in London's care homes: the effect of passive ventilation. International Building Performance Simulation Association (IBPSA).
UK Health Security Agency, 2022. Heat mortality monitoring report: 2022. https://www.gov.uk/government/publications/heat-mortality-monitoring-reports/heat-mortality-monitoring-report-2022#:~:text=Summer%202022%20was%20an%20exceptional,least%20one%20region%20in%20England. Accessed: 2023-08-22.
UK Health and Security Agency, 2023. Looking after children and those in early years settings before and during hot weather: teachers and other educational professionals. https://www.gov.uk/government/publi2cations/hot-weather-and-health-supporting-vulnerable-people/looking-after-children-and-those-in-early-years-settings-during-heatwaves-for-teachers-and. Accessed: 2023-09-28.
US Department of Energy, 2021. Energyplus version 9.6.0 input output reference. https://energyplus.net/assets/nrel_custom/pdfs/pdfs_v9.6.0/InputOutputReference.pdf. Accessed: 2023-08-23.
Wargocki, P., Porras-Salazar, J.A., Contreras-Espinoza, S., 2019. The relationship between classroom temperature and children's performance in school. Build. Environ. 157, 197–204.
Williams, K.D., et al., 2017. The met office global coupled model 3.0 and 3.1 (GC3 & GC3.1) configurations. J. Adv. Model. Earth Syst. 10, 357–380.
Wood, S.N., Pya, N., Safken, B., 2016. Smoothing parameter and model selection for general smooth models. J. Am. Stat. Assoc. 111, 1548–1563.
Zennaro, F., Furlan, E., Simeoni, C., Torresan, S., Aslan, S., Critto, A., Marcomini, A., 2021. Exploring machine learning potential for climate change risk assessment. Earth Sci. Rev. 220, 103752.